11. TITAN-I DIVERTOR ENGINEERING

Patrick I. H. Cooke
Edward T. Cheng
Steven P. Grotz
Charles C. Bathke
Richard L. Creedon
Mohammad Z. Hasan
Shahram Sharafat
James P. Blanchard
William P. Duggan
George E. Orient

Contents

11. TITAN-I DIVERTOR ENGINEERING

11.1. INTRODUCTION

This section describes the engineering design of the divertor of TITAN-I, including the thermal and mechanical design of the divertor components, materials selection, and fabrication issues. Toroidal-field divertors are selected as the impurity-control and particle-exhaust system of TITAN reactors. An account of the magnetics analysis for the divertor is contained in Section 4.4, and the edge-plasma and neutral-particle modeling, which had a strong bearing on the engineering of the divertor, are described in Sections 5.4 and 5.5, respectively.

The design of the impurity-control system poses some of the most severe problems of any component of a DT fusion reactor. For TITAN the divertor design probably represents (perhaps together with the design of the oscillating-field current-drive system, described in Section 7) the most critical engineering and physics issue for the reactor. Even low-power-density devices such as NET [1], operating at a neutron wall loading of about $1\,MW/m^2$, encounter major problems in the design of in-vessel components. Although the differences in configuration between poloidal divertors in tokamaks and toroidal divertors in reversed-field-pinch (RFP) reactors make a direct comparison difficult, the particle and heat loadings on the divertor might be expected to scale with the neutron wall loading, implying that the divertor conditions for the TITAN divertor might be a factor of about 20 more severe than for NET, all other things being equal. Therefore, special attention was given to this aspect of the TITAN design. The final divertor design is the result of extensive iteration between the magnetic design, edge-plasma analysis, thermal and mechanical design, and divertor-plate fabrication issues.

The two main design issues for the divertor system are to achieve heat loadings on the divertor collector plate (or target) that do not exceed the maximum acceptable level, while simultaneously ensuring that the sputtering erosion rate does not lead to an early failure of the component. These two aims tend to conflict, because the high heat loadings which inevitably occur on the divertor target require the use of thin structures to minimize temperature differences and thermal stresses, while a thick structure is necessary to give a long life against erosion.

A summary of the results of the edge-plasma modeling is given in Table 11.1-I and are described in detail in Section 5.4. The plasma power balance is controlled by the

Table 11.1-I.

SUMMARY OF TITAN-I EDGE-PLASMA CONDITIONS

Number of divertors(a)	3	
Scrape-off layer thickness	6	cm
Peak edge density	1.7×10^{20}	m^{-3}
Peak edge ion temperature	380	eV
Peak edge electron temperature	220	eV
Plasma temperature at first wall	1.7	eV
Peak divertor density	6×10^{21}	m^{-3}
Peak divertor plasma temperature	4.5	eV
Divertor recycling coefficient	0.995	

(a) Toroidal divertor (poloidally symmetric) with "open" geometry.

injection of a trace amount of a high atomic number impurity (xenon) into the plasma, causing strong radiation from the core plasma, the scrape-off layer (SOL) plasma, and the divertor plasma. About 95% of the steady-state heating power (alpha particle and ohmic heating) can be radiated to the first wall and divertor plate, with about 70% being radiated from the core plasma (*i.e.*, inside the separatrix). This intense radiation reduces the power deposited on the divertor target by the plasma to an acceptably low level. Preliminary experimental results suggest that beta-limited RFP plasmas can withstand a high fraction of power radiated without seriously affecting the operating point (Section 5.3); this behavior contrasts with that observed in tokamaks, in which a high radiation fraction appears to lead to a plasma disruption. The radiative cooling also reduces the electron temperature at the first wall and divertor target (also assisted by recycling) which, in turn, reduces the sputtering erosion problem.

As discussed in Section 4.4, the TITAN divertor uses an "open" configuration, in which the divertor target is located close to the null point, facing the plasma, rather than in a separate chamber. This positioning takes advantage of the increased separation

between the magnetic field lines (flux expansion) in this region, which tends to reduce the heat loading on the divertor plate because the plasma flowing to the target is "tied" to the field lines. The high plasma density in front of the divertor target ensures that the neutral particles emitted from the surface have a short mean free path; a negligible fraction of these neutral particles enter the core plasma (Section 5.5).

The TITAN-I divertor coils are based on the integrated-blanket-coil (IBC) concept [2], in which an electrical current flows in a liquid-lithium coil, thereby combining the functions of magnetic-field production, tritium breeding, and heat removal in a single system. This approach also reduces the need to shield the divertor coils significantly.

The magnetics design (Section 4.4) focussed on maximizing the achievable degree of flux expansion, in order to minimize the peak heat flux on the divertor target while minimizing the divertor coil currents, since the ohmic losses in the divertor IBC represent a large fraction of the recirculating power in the reactor. The final magnetics design includes three divertor modules which are located 120° apart in toroidal direction. An equatorial-plane cross section of the coils is shown in Figure 11.1-1. The magnetic-field lines are diverted onto the divertor plate using a nulling coil and two flanking coils, with the latter localizing the nulling effect. For the TITAN-I design, the divertor IBC assembly displaces a part of the toroidal-field (TF) IBC tube bank. Therefore, a pair of trim coils is also required to control the toroidal-field ripple; the trim coils are also IBCs.

11.2. MATERIALS

11.2.1. Plasma-Facing Material

In order to reduce the erosion of the divertor armor by the plasma, a high atomic-number (Z) material must be used for the surface of the divertor plate. This conclusion is based on the estimates of sputtering rates of various candidate materials (described in Section 5.5). The threshold energy for sputtering is sufficiently high for high-Z materials, that the erosion rate of the divertor target under the expected conditions for TITAN designs (Table 11.1-I) is acceptable.

Various high-Z materials were considered for the divertor target. Molybdenum has excellent physical properties as well as good resistance to sputtering damage, but suffers from serious activation when exposed to a fusion-neutron energy spectrum. Tantalum also has good thermal and mechanical properties and is relatively easy to fabricate into complex components. However, tantalum absorbs large quantities of hydrogen in the

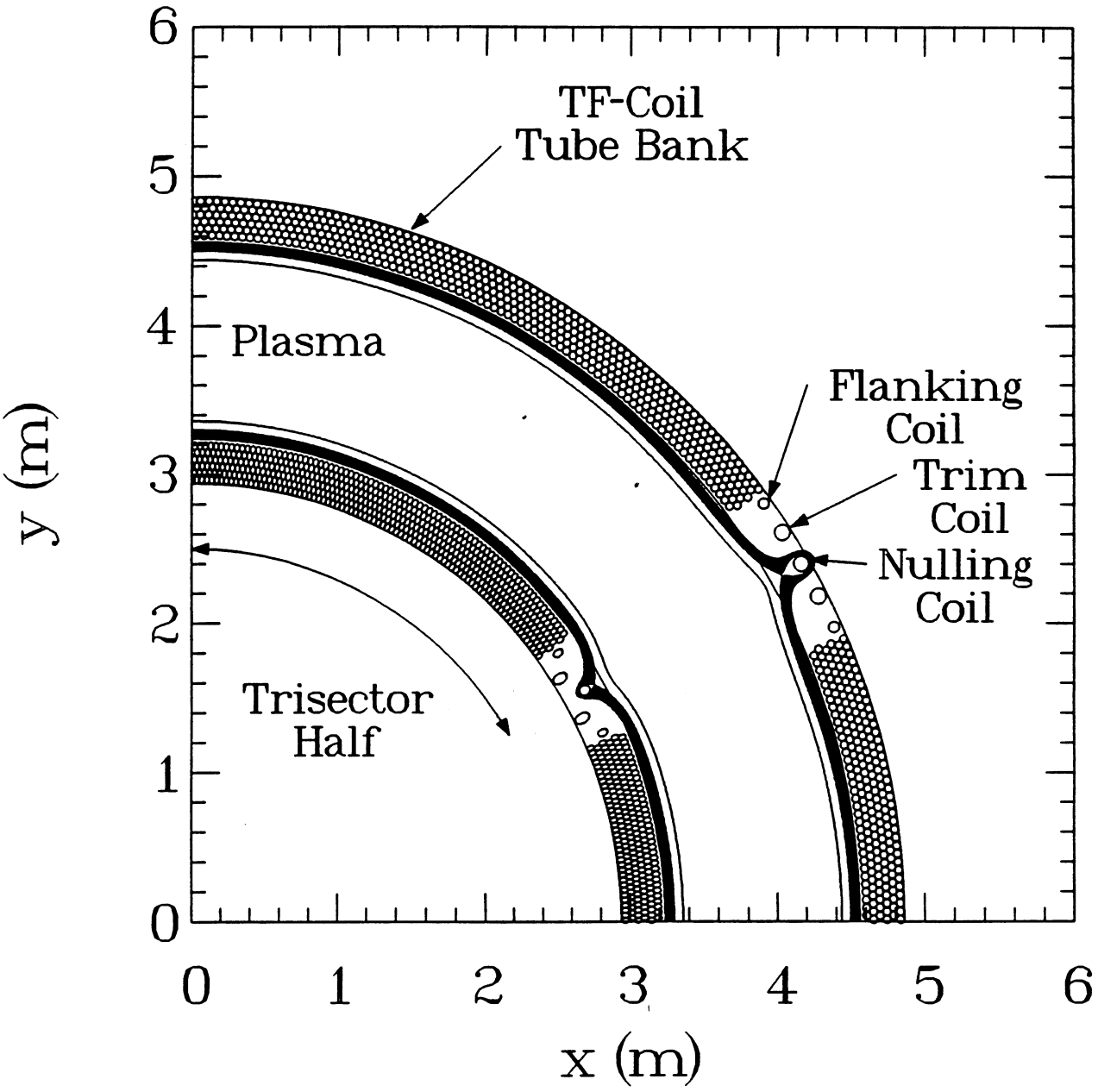

Figure 11.1-1. Equatorial-plane view of divertor coils and magnetic-field lines for TITAN-I, showing TF and divertor IBCs.

temperature range of interest ($\sim$ 300-800 °C), which causes an embrittlement problem [3, 4]. Tungsten has good thermal and mechanical properties which are retained at high temperatures, and also has a very low sputtering rate, which has led to the specification of a 2-mm-thick armor to ensure a one-year lifetime. One of the inherent problems with unalloyed tungsten is the lack of ductility (brittleness) at room temperature. Addition of rhenium results in a tungsten alloy that combines the high-temperature strength of pure tungsten with useful room-temperature properties in both the stress-relieved and recrystallized conditions [5].

Maykuth *et al.* [6] reviewed the workability and mechanical properties of tungsten alloys containing rhenium. The elevated-temperature properties of the recrystallized W-27Re and W-30Re alloys are shown in Figure 11.2-1. Generally, the maximum effect of rhenium in improving mechanical properties of refractory metals is obtained with the maximum amount of rhenium which can be retained in solid solution. However, rhenium solubility decreases with temperature, and tungsten alloys containing 27% or more rhenium are subject to precipitation of the hard and brittle σ phase at low temperatures [6]. On the other hand, the mechanical properties of tungsten are not significantly influenced for rhenium contents smaller than 3% [7]. For these reasons, the useful rhenium content range in tungsten-rhenium alloys is generally 3-27 at.%.

Another issue is the high ductile-to-brittle transition temperature (DBTT) for pure tungsten, below which tungsten is extremely brittle and cannot be worked. Pure tungsten has a DBTT of about 200 to 400 °C depending on the impurity content, thermomechanical history, and thickness [7]. The addition of rhenium reduces the DBTT appreciably. The DBTT of W-26Re alloy is about 90 °C [7] which is a great improvement over pure tungsten. Forming, cutting, milling, and drilling of W-26Re alloy must be done at temperatures well above 90 °C DBTT. Therefore, if the application requires tungsten with ductility at room temperature and/or ductility after operating above recrystallization temperature, the W-26Re alloy is a logical choice. It should also be selected if the fabrication of the part is unusually difficult. Weldments made with W-26Re are ductile, unlike unalloyed tungsten weldments which always recrystallize the metal and hence are brittle [8].

The properties of the W-26Re alloy are described in Section 11.2.4 and summarized in Table 11.2-I. The primary drawback of W-Re alloys is the cost of rhenium which ranges from $800 to $1500 per pound [8]. A further issue is the activation of rhenium and its impact on the rad-waste disposal which is reported in Section 13.7.

The data base of neutron-irradiation effects on tungsten and its alloys is very sparse. Further research on the irradiation behavior of W-Re alloys is needed to establish lifetime-

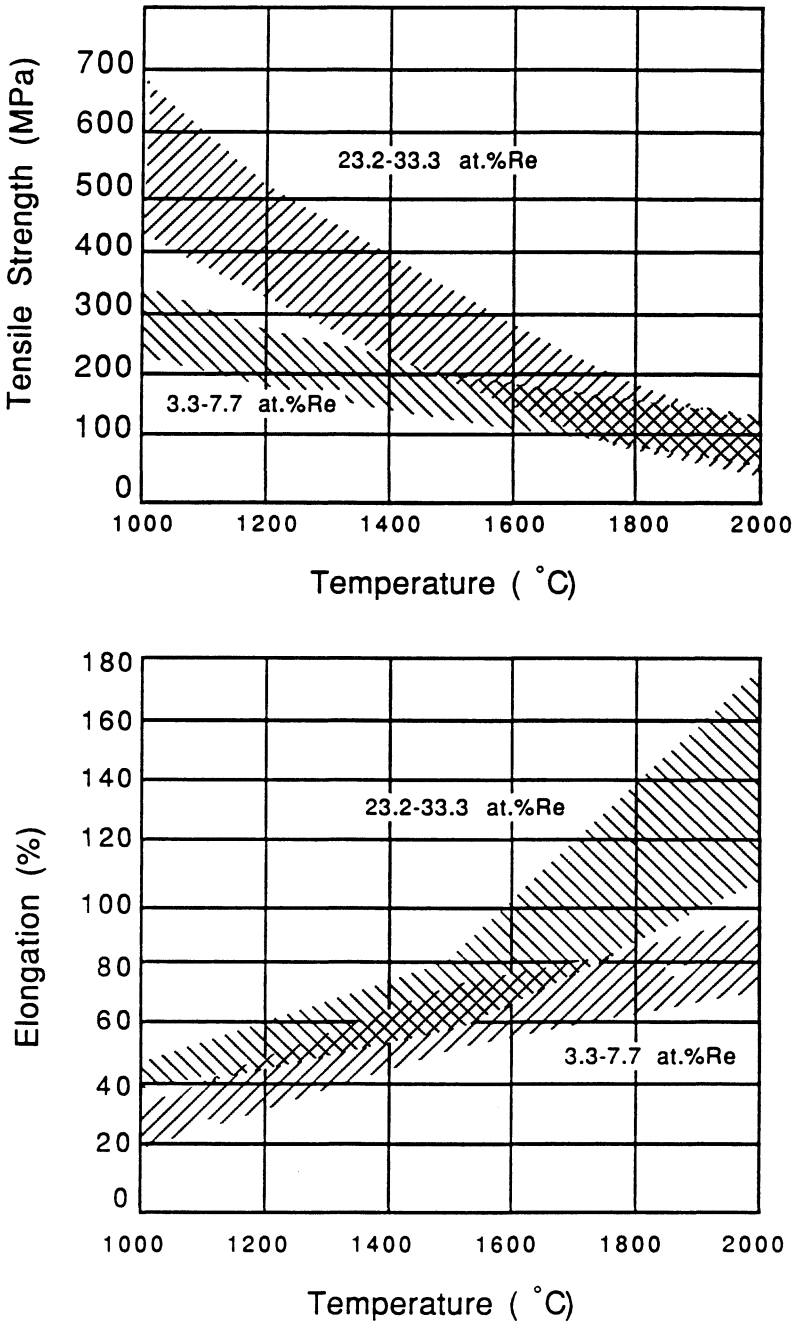

Figure 11.2-1. Ultimate strength and elongation as functions of temperature for W-Re alloys in the recrystallized condition [6]

Table 11.2-I.

SELECTED PROPERTIES OF W-Re [7], V-15Cr-5Ti, Al_2O_3, AND $MgAl_2O_4$

PROPERTY	W-26Re	W-3Re	V-15Cr-5Ti	Al_2O_3	$MgAl_2O_4$
Melting temperature (°C)	3,180	3,180	1,890	2,050	2,135
Linear thermal-expansion coefficient (10^{-6}/ °C)					
500 °C	7.06	4.48	10.3	7.8	8.
1,000 °C	7.95	5.14	11.1	–	9.
Thermal conductivity (W/m°C)					
600 °C	–	–	27.5	9.1	8.1
1,000 °C	66.72	99.[a]	29.	–	6.
2,000 °C	62.82	136.[a]	–	–	–
Recrystallization temperature (°C)					
Incipient after 1 h anneal	1,500	1,400	< 1,100	–	–
Complete after 1 h anneal	1,650	–	–	–	–
DBTT (°C)	90	< 150[b]	< 0	–	–
Electrical resistivity ($\mu\Omega$m)					
20 °C	–	0.092	0.39	$> 10^{20}$	$> 10^{20}$
500 °C	0.35	0.18[a]	0.74	$> 10^{16}$	$> 10^{16}$
1,000 °C	0.55	0.33[a]	1.[c]	$> 10^{12}$	$> 10^{12}$
2,000 °C	0.85	0.65[a]	–	–	–
Tensile strength (MPa)					
600 °C	–	–	300	235	250
1,000 °C	450-680	240-320	250[d]	–	–
1,500 °C	200-340	110-190	–	–	–
2,000 °C	30-110	40-100	–	–	–
Modulus of elasticity (GPa)					
20 °C	430	410[a]	127	–	–
1,000 °C	380[c]	360[a]	115	–	–
Elongation (%)[e]					
650 °C	30	–	10-20	–	–
1,000 °C	39-45	20-30	–	–	–
1,500 °C	60-80	50-70	–	–	–
2,000 °C	110-170	70-100	–	–	—

(*a*) Pure tungsten values.

(*b*) DBTT for pure tungsten is in the range 100-400 °C.

(*c*) Estimated values.

(*d*) Value at 900 °C.

(*e*) Data from Reference [6].

limiting factors in a neutron environment. Lastly, the relatively large afterheat in the tungsten armor of the divertor plate should be considered in the safety design of the reactor (Section 13).

11.2.2. Divertor-Target Coolant

The natural choice for the coolant of high heat-flux components is water but, for the lithium-cooled FPC of TITAN-I, fundamental safety considerations prohibit the use of water anywhere within the containment building (Section 13). Gaseous coolants, such as helium, were considered, but removing high heat fluxes is possible only at a low coolant temperature and requires large pumping powers.

Lithium cooling of the divertor target is an attractive option because it enables the divertor cooling circuit to be integrated with that of the first wall, blanket, and shield. Generally, the MHD effects make liquid-metal cooling of high heat-flux components such as divertors and limiters difficult. The magnetic topology of the RFP, however, makes this option viable. Since the toroidal component of the magnetic field near the first wall is small for the RFP ($\sim 0.4\,\mathrm{T}$ for TITAN), only a relatively minor pressure drop is encountered by a poloidally flowing coolant; for the toroidal divertor used in TITAN-I this problem is further eased because of the reduction of the toroidal-field strength in the vicinity of the null point.

For these reasons, lithium was chosen as the divertor-target coolant for the TITAN-I design. The thermal-hydraulic calculations and the integration of the divertor and first-wall coolant circuits are described in Section 11.4.

11.2.3. Substrate Material

There is a strong incentive to design a divertor target using a single material to eliminate the problems of bonding dissimilar materials, differential thermal expansion, and additional stresses at the interface of the different materials. It is desirable, therefore, to use W-Re alloy for both the divertor substrate and coolant tubes since manufacturing W-Re tubes using powder metallurgical techniques is possible using current technology (as proposed for TITAN-II in Section 17). The high electrical conductivity of the W-Re tubes, however, would produce a large MHD pressure drop. For this reason, the same vanadium alloy (V-3Ti-1Si) is used for the divertor substrate as was used for the structural material of the first wall. Relevant physical properties of V-15Cr-5Ti, which are similar

to those of V-3Ti-1Si alloy, are listed in Table 11.2-I. The effects of neutron irradiation on the vanadium-base alloys are also discussed in Section 10.2. Detailed fabrication techniques for the divertor target and joining of the vanadium-alloy tubes to the tungsten-alloy armor are discussed in Section 11.3.

11.2.4. Insulator Material

If a good electrical contact exists between the coolant tubes and the armor, then the higher conductivity of the tungsten-rhenium armor will produce a larger MHD-induced pressure drop than would occur with bare vanadium tubes. Therefore, the coolant tubes of the TITAN-I divertor are electrically insulated from the armor by a thin layer of spinel ($MgO\text{-}Al_2O_3$), which has a high resistance to radiation damage and a relatively high thermal conductivity ($\sim 8\,W/m\,K$). This method of insulation is preferred over the use of an insulator inside the tube, which would lead to the undesirable exposure of the insulator to the high-velocity lithium coolant. Furthermore, the use of laminated tubes would pose fabrication problems for the small tubes employed in the TITAN-I divertor. Selected properties of spinel are also given in Table 11.2-I.

In addition to reducing the MHD pressure drop, the use of spinel as the insulating material introduces another highly desirable characteristic. Experiments on hydrogen permeation through nonmetallic solids have concluded that Al_2O_3 has about two to three orders of magnitude lower hydrogen permeability than the least permeable of the refractory metals [9]. Hydrogen permeability behavior of spinel is expected to be similar to that of pure alumina (Al_2O_3). The low permeation rate of hydrogen through spinel has an important impact on the tritium inventory in the divertor target and on the tritium extraction system because the divertor target is exposed to high particle fluxes.

11.2.5. Compatibility

A schematic cross section through the divertor target, showing the various materials, is given in Figure 11.2-2. The use of three different materials in the TITAN-I divertor plate requires that these materials be compatible with each other. They need to be chemically stable with respect to each other and have matching mechanical properties. The most significant properties are thermal conductivity and thermal-expansion coefficients. Adequate thermal conductivity reduces thermal stresses and similar expansion coefficients reduce mismatch stresses at interfaces. Table 11.2-I lists selected properties

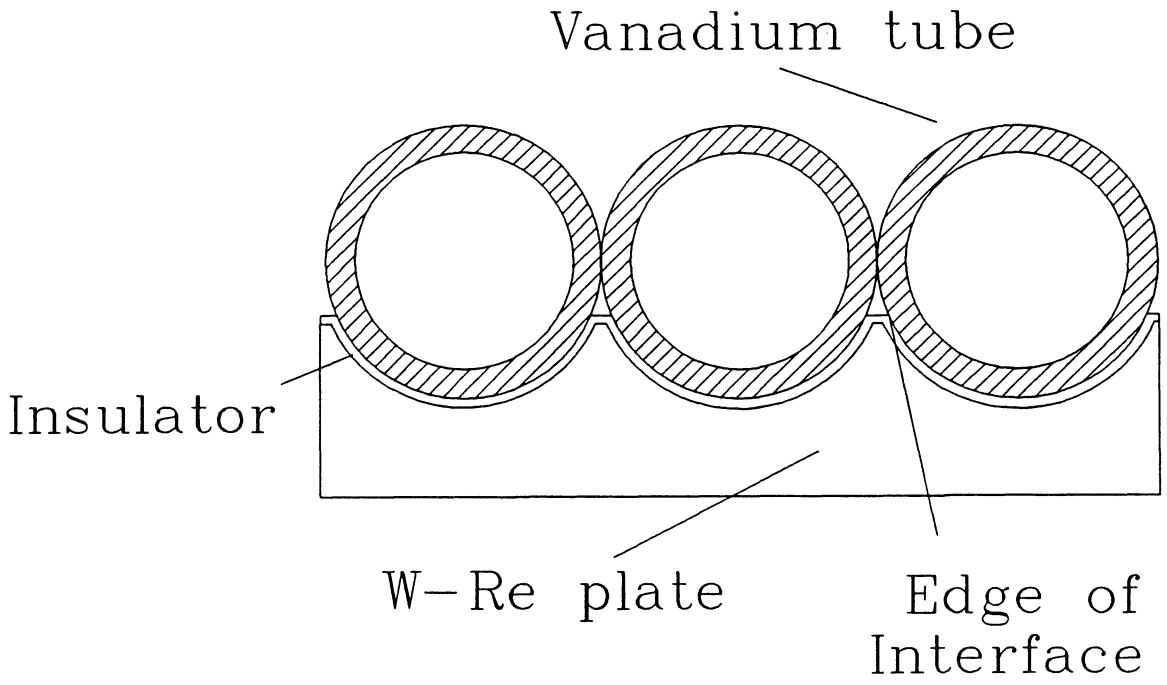

Figure 11.2-2. Schematic cross section through divertor target of TITAN-I, showing the coolant tubes, the spinel insulator layer, and the W-Re divertor target.

of the three candidate materials for the TITAN-I divertor plates. The linear thermal-expansion coefficient of the armor (W-26Re), the substrate (V-15Cr-5Ti or V-3Ti-1Si), and the insulator (spinel) match closely.

Even though the thermal conductivity of spinel is greater than that of most insulator materials, it is still much less than that of the vanadium or tungsten alloys. However, the insulating film between the tungsten-rhenium plate and the vanadium tubes is only a few μm thick and, therefore, only a relatively small temperature drop will appear across the spinel despite its poor thermal conductivity.

The chemical compatibility of spinel with tungsten-base and vanadium-base alloys has been investigated. Tungsten-base alloys are often used in combination with ceramic furnace materials (*e.g.*, Al_2O_3, MgO, graphite, BeO, ThO_2, and ZrO_2). The Plansee Corporation [7] has established maximum operating temperatures for tungsten in contact with these furnace materials. Typical maximum operating temperatures for graphite, Al_2O_3, and MgO are, respectively, 1400, 1500, and 1900 °C. The maximum operating temperature of the tungsten-rhenium plates in contact with spinel will likely be between the two latter limits (*i.e.*, 1500-1900 °C).

The compatibility of spinel and vanadium-base alloys has been studied in detail [10, 11]. The standard free energy of formation for spinel is about one half of that of vanadium oxides in the temperature range of 500 to 1500 °C. Therefore, using spinel as an insulating film in contact with vanadium should not pose a compatibility problem.

The effects of neutron irradiation on the spinel insulating material are discussed in Section 10.2. Spinel swells to a few percent of original volume depending on the operating temperature and is shown to be most susceptible in the 150 to 300 °C range, which is well below the anticipated operating temperature for the spinel insulating film in the TITAN-I divertor plate.

11.3. TARGET FABRICATION

The TITAN-I divertor plates are cooled with liquid lithium. The high electrical conductivity of tungsten requires electrical insulation of the target plate from the coolant tubes to reduce MHD pressure drops. Several fabrication procedures for the TITAN-I divertor target were investigated. In cooperation with the Plansee research and development group [12], the following four-step fabrication procedure was identified as feasible:

- Manufacture the W-Re plate using powder metallurgy;
- Mill the W-Re plate for coolant-tube grooves;
- Chemical-vapor deposit the electrical insulator;
- Braze the vanadium coolant tubes to the W-Re plate.

Manufacturing the W-Re plate using powder metallurgy (PM). Tungsten powder is usually produced by reduction of tungsten oxides using high temperature hydrogen (1000 °C). The tungsten powder is then pressed hydraulically or isostatically into rods, plates, or other shapes. The pressed compact is then sintered in high purity hydrogen at 2500 °C into a "pressed and sintered" ingot having a density of about 92%. Alloying elements are introduced into the powder before the high-temperature sintering takes place.

The Plansee manufacturing plant routinely produces tungsten-base-alloy sheets of up to 100 cm and up to 7 mm thick [7,8]. Thus fabrication of a $2 \times 150 \times 5,000$ mm continuous W-Re plate (TITAN-Idivertor plate) can be considered a routine procedure.

Milling of the W-Re plate for coolant tube grooves. The next step in the divertor-plate fabrication is milling of coolant grooves along the plate. Tungsten-base alloys can be folded, bent, formed, spun, sheared, stamped, punched, riveted, ground, and machined (*i.e.,* turned, milled, or drilled [8]).

Chemical-vapor deposition (CVD) of the electrical insulator. The CVD process is very versatile in depositing a large variety of elements and compounds at relatively low temperatures (400-800 °C). A unique feature of CVD is the control of stoichiometric composition and layer structures which is difficult or impossible to attain by other techniques. The CVD process involves chemical or thermal decomposition of gaseous species at a hot susceptor surface. Stringent quality requirements can be achieved by controlling temperature, pressure, and gas-flow rates of species and cover gases. Therefore, CVD has become a cornerstone for modern technologies such as solid-state electronics. Routinely applied CVD materials include [13]:

- Insulators (SiO_2, Al_2O_3, $MgAl_2O_4$, TiO_2, Nb_2O_5),
- Conductors (W, W-Re, W-Mo-Re, Ta-W, V),
- Superconductors (Nb_3Ge),
- Transparent conductors (VO_2, V_2O_5, SnO_2, In_2O_3),
- Semiconductors (Group II - Group VI).

One of the greatest advantages of the CVD process is that gradual material changes of the deposited compound are possible. For the divertor plate, the CVD process can start with the deposition of W-Re onto the W-26Re plate. By gradually changing the gaseous composition, the deposition of W-Re can be changed into deposition of spinel.

Brazing of vanadium coolant tubes to the spinel-insulated W-Re plate. Joining of refractory alloys by welding is generally not preferred, because embrittlement of the weldment may occur. Although W-26Re does show retention of ductility of weldments, brazing is preferred because the vanadium tubes must be joined to the spinel insulating film. The Plansee Corporation has evaluated and developed a series of brazing materials for joining various refractory metals and alloys. As long as the braze material has a melting point below the recrystallization temperature of the tungsten- or the

vanadium-base alloy, embrittlement can be avoided. Recrystallization of W-26Re sets in at around 1500 °C while for the vanadium alloy, recrystallization can start between 800 to 1100 °C (Section 10.2). Table 11.3-I lists some of the commercially used brazing materials developed by Plansee [7].

Table 11.3-I.

BRAZING MATERIALS FOR REFRACTORY METALS [7]

Material	Brazing Temperature (°C)
Rhodium	1970
PtPd20Au5	1695-1645
Palladium	1550
Nickel	1430
AuPd25	1410-1380
AuPd13	1305-1260
CuNi45	1300
PdNi	1240
CuNi30	1230
AgPd33Mn3	1200-1180
NiMn31Pd21	1120
AgPd20Mn5	1120-1000
CuPd18	1090-1080
AgPd5	1010-970
AgCu20Pd15	900-850

11.3.1. Ceramic-Metal Adhesion

The main concern regarding the divertor plate performance is the integrity of the bond between the tungsten-rhenium armor plate and the vanadium tubes with a thin, ceramic insulating material sandwiched between. The adhesion at ceramic-metal interfaces has always been a concern for industries developing hard, wear-resistant coatings such as carbides and nitrides of tungsten, tantalum, and titanium on soft and ductile substrates. Ceramic-metal interfaces are used extensively by the electronics industry and are also heavily employed in rockets and jet-turbine components. A few examples of latest findings of ceramic-metal interface integrity follow.

Extensive research began in the late 1960s on CVD of insulator and composite structures. Various combinations of metal-ceramic-metal insulating "tri-layer sandwich" structures of W, W-Re, Nb, and Mo were fabricated by the CVD process. Aluminum oxide, hafnium oxide, and zirconium oxide were the primary insulating material. Tubular structures of these sandwich composites were cycled between 1300 °C and room temperature without any apparent damage to the oxide layer or either of the oxide-metal bonds [14]. Extended-length thermocouple wires made of W-Re were routinely coated with hafnium-oxide insulation and used as temperature probes measuring up to 2500 °C [14].

Recently the solid-state bonding of oxide ceramics to steels was studied to examine the bonding strength and the resistance to thermal cycling for alumina-steel joints [15]. A series of metallic interlayers of various thicknesses between the ceramic and the steel were examined. It was found that using a thin (1 mm) metallic interlayer of Nb-Mo produces a superb bond between the oxide and the steel with a strength of 450 to 500 MPa, as measured in a four-point bending test, which corresponds to the strength of the alumina. The Nb-Mo interlayer also proved superior to others in withstanding the effects of thermal expansion mismatches at the joints and in resisting thermal cycling between room temperature and 500 °C.

Research by the electronics industry into improvements of ceramic-metal bonds has recently lead to new discoveries. Adhesion enhancement of a film of nonreactive metal deposited on a ceramic or glass substrate can be produced by irradiating the interface with an ion beam [16]. This method produced thermally stable, adhesion-strength characteristics of chemical bonding for metal films on the surfaces of ceramics. The superior strength achieved was attributed to "interface mixing" of interface atoms. Although the mechanism responsible for the superior bonding strength is not fully understood it is postulated that ion-beam irradiation produces a preferred organization of the atom species that minimizes the interface energy.

Based on the above observations, an alternate technique for the fabrication of the TITAN-I divertor is possible using a gradual CVD mechanism. This CVD process starts with the deposition of W-Re onto the W-26Re plate. By gradually changing the gaseous composition, the deposition of W-Re can be changed into deposition of spinel. After the desired spinel thickness has been achieved, deposition of vanadium can be introduced gradually. This process eliminates sudden changes in material properties resulting in better adherence and improved resistance to film delamination. It is speculated that this gradual compound-deposition mechanism would result in both above-mentioned enhancement processes (*i.e.*, a metallic interlayer and "interface mixing").

11.3.2. Discussion

The feasibility of using tungsten-rhenium for the divertor armor is no longer seen as an issue. High-ductility tungsten-rhenium alloys have been developed since the mid 1950s and show promising properties for fusion applications. Tungsten-rhenium alloys have appreciably lower DBTT when compared to pure tungsten. Because the TITAN-I divertor plates are cooled with liquid lithium, electrically insulated V-3Ti-1Si coolant tubes have to be used. Highly radiation-damage-stable spinel is proposed as the insulating material.

The fabrication process of a divertor plate made from two different materials brazed together with a thin electrical insulating film between them has been discussed. As a second technique, a unique manufacturing process using CVD is proposed to enhance bond strength of the tungsten-spinel-vanadium interfaces. An extensive research and development effort is needed to establish the manufacturing feasibility and performance characteristics of such a system.

11.4. TARGET DESIGN

The materials considerations described in the previous section led to the basic layout of the divertor target shown in the schematic cross section in Figure 11.2-2. The details of the shaping of the surface and the overall thermal analysis are described in this section; a more extensive structural and thermal analysis using finite-element techniques is reported in Section 11.5.

11.4.1. Target Shaping

Despite the intense radiation resulting from the impurities injected into the plasma, careful shaping of the divertor target is required to maintain the heat flux at acceptable levels at all points on the plate. Various factors combine to complicate the shaping problem.

The heat flux associated with the plasma flow on to the target depends nonlinearly on the location in the scrape-off layer and the inclination angle of the target with respect to the field lines. Heating by plasma radiation is taken from the edge-plasma transport analysis performed by the edge-transport code ODESSA (Section 5.4), and is divided into two sources: an upstream zone (the edge plasma, or scrape-off layer) and a downstream zone (the divertor plasma). The former component of radiation is analogous to the surface heating on the first wall and varies with the angle of the target with respect to the centerline of the core plasma. The downstream radiation varies with the local plasma properties and, as the radiating zone is spread over a finite volume, it is assumed that only 25% of this heating is deposited locally on the target; the remainder goes to the first wall.

The heat flux from the plasma and the downstream radiation is directly affected by the local spacing between the magnetic field lines. In order to calculate these heating rates, it is necessary to determine the flux-expansion factor, defined as the ratio of the value of the local magnetic field (toroidal and radial) to the field at a point between two divertors on the same field line (Section 4.4). This factor changes rapidly in the vicinity of the divertor null point.

A further complication arises from the liquid-metal cooling of the target. For a given pressure drop along the coolant path, MHD effects will cause the coolant velocity to adjust according to the local value of the magnetic field. Because the heat-transfer coefficient is a function of the coolant velocity, the allowable heat flux varies with position along the target.

These considerations require an iterative procedure for the divertor design. A guess for the shaping for the target surface is made, and the heat-flux distribution for this shape is calculated to allow a thermal-hydraulics analysis for the target cooling to be performed. If any of the constraints imposed on the thermal design (especially the maximum temperature limits for the various materials) is exceeded, then the shaping is adjusted until an acceptable solution is obtained.

The above iterative procedure has been simplified by writing a computer code to perform the thermal analysis. This code produces an approximation to the profile of the

target in 3-D by specifying its shape in both the inboard and the outboard intersections with the equatorial plane (the two sets of field lines in Figure 11.1-1). It is assumed that the full shape of the target is completed by a smooth curve along the poloidal direction between the two sets of points thus created, and that the values of quantities such as magnetic field strength and heat flux, vary smoothly between their values at these two inboard and outboard locations.

The target-shape profile is described by the coordinates of a number of points where field lines intersect the surface of the target. The input for the code takes the form of this set of coordinates on the target, together with values of heat flux (taken directly from the ODESSA code), magnetic field strength, inclination angle of the target, and flux-expansion factor, at each point.

11.4.2. Target Thermal-Hydraulic Design

The surface heat flux on the target, q''_{sur}, is given by

$$q''_{sur} = q''_1 + q''_2 + q''_3 , \tag{11.4-1}$$

where

$$q''_1 = \frac{\sqrt{B_\phi^2 + B_r^2}}{B_\theta} q''_{\|} \frac{\sin\alpha}{f_{exp}} , \tag{11.4-2}$$

$$q''_2 = \frac{\sqrt{B_\phi^2 + B_r^2}}{B_\theta} q''_{d,rad} f_{d,rad} \frac{\sin\alpha}{f_{exp}} , \tag{11.4-3}$$

$$q''_3 = \frac{f_{RAD}\,(P_\alpha + P_\Omega)}{A_{FW}} \sin\beta \frac{r}{r_{FW}} , \tag{11.4-4}$$

are the components of the surface heat flux from the plasma particles, radiation from the divertor plasma, and radiation from the edge plasma, respectively. In these expressions, $q''_{\|}$ is the parallel plasma heat flux along the field line, $q''_{d,rad}$ is the radiation from the divertor plasma converted to a parallel plasma heat flux, and $f_{d,rad}$ is the fraction of the divertor plasma radiation which is assumed to be locally deposited on the target. The magnitude of the toroidal, poloidal, and radial magnetic fields are, B_ϕ, B_θ, and B_r, respectively, and $\sqrt{B_\phi^2 + B_r^2}/B_\theta$ represents the pitch of the field line. The inclination angle of the target with respect to the field line is α, f_{exp} is the flux-expansion factor, and f_{RAD} is the radiation fraction from the core and edge plasmas (the fraction of the alpha, P_α, and ohmic, P_Ω, heating powers which is radiated). The area of the first wall

is A_{FW}, β is the angle of the target with respect to the plasma centerline, r is the local value of minor radius, and r_{FW} is the minor radius of the first wall.

The total coolant pressure drop, ΔP, was calculated from the equation

$$\Delta P = \sigma_f v B_\perp^2 L \frac{\phi}{1+\phi} + \sigma_f v B_\parallel^2 d_i \sqrt{\phi} + 0.1\sigma_f v B_\parallel^2 d_i \sqrt{\phi} + f L \frac{\rho v^2}{2 d_i}, \quad (11.4\text{-}5)$$

with ϕ given by

$$\phi = \frac{\sigma_w t_w}{\sigma_f r_i}, \quad (11.4\text{-}6)$$

where σ_f and σ_w are the electrical conductivities of the coolant and tube wall, respectively, L is the length of the coolant tube, d_i and r_i are, respectively, the inner diameter and inner radius of the coolant tube, and t_w is the tube-wall thickness. The parallel and perpendicular magnetic field strengths are, respectively, $B_\parallel$ $(= B_\theta)$ and $B_\perp$ $(= \sqrt{B_\phi^2 + B_r^2})$. The parameter f is the friction factor, ρ is the coolant density, and v is its velocity. In the pressure drop equation, the first term is the MHD pressure drop resulting from the coolant flow along the length of the tube in the poloidal direction. The second and third terms represent, respectively, the pressure drop caused by the bends and by the gradient of the poloidal field. For these calculations, the magnetic field values are averaged between the inboard and outboard locations. The final term in Equation 11.4-5 gives the usual frictional pressure drop. A detailed justification for the use of these equations is given in Section 10.4.

Since the divertor coolant tubes are all fed from the same circuit, the total pressure drop, ΔP, is specified. It is desirable that this pressure drop be close to that of the first-wall coolant circuit so that both systems can be fed from the same coolant circuit. A constraint on the maximum velocity of coolant in the divertor tubes was also imposed. Given the total pressure drop, Equation 11.4-5 was solved to find the coolant velocity in each tube. For certain tubes, the resultant velocity exceeded the imposed maximum-velocity constraint. For these tubes, the pressure drop should be lowered; the pressure drop between inlet and outlet of these tubes was calculated from Equation 11.4-5 using the maximum-velocity limit. It was assumed that flow orificing would provide the difference between the pressure drop on the circuit and the pressure drop between inlet and outlet of these selected tubes.

A higher surface heat flux can be accommodated by using turbulent coolant flow which is accompanied by a higher Nusselt number compared with that of a laminar flow. The low value of the perpendicular (toroidal and radial) magnetic field in the RFP allows

the possibility of the liquid-metal coolant flow entering the turbulent regime. The flow is turbulent if

$$Re \;>\; 60\, H_{\|} \,. \tag{11.4-7}$$

Otherwise, the flow is laminar (Section 10.4). In Equation 11.4-7, Re is the Reynolds number ($Re = \rho v d_i/\eta$, and η is the coolant viscosity), and $H_{\|}$ is the parallel Hartmann number ($H_{\|} = d_i\, B_{\|} \sqrt{\sigma_f/\eta}$).

The Nusselt number, Nu, is given by

$$Nu \;=\; \begin{cases} 6 & \text{laminar} \\ 6.5 + \dfrac{0.005 Pe}{1 + 1890 (H_{\|}/Re)^{1.7}} & \text{turbulent} \end{cases} , \tag{11.4-8}$$

where Pe is the Peclet number of the coolant ($Pe = Re\, Pr$, and Pr is the Prandtl number). In determining the heat transfer coefficient, h ($= k_f Nu/d_i$, and k_f is the thermal conductivity of the coolant), the value of the Nusselt number from Equation 11.4-8 is halved to account for the effects of nonuniform heating around the circumference of the tube.

The coolant outlet temperature, T_{ex}, is computed from the energy balance equation

$$T_{ex} \;=\; T_{in} + \frac{d_o\, q''_{sur} + \frac{\pi}{4}\,(d_o^2 - d_i^2)\, q'''_w + d_o \left[t_a + d_o \left(\frac{1}{2} - \frac{\pi}{8}\right)\right] q'''_a + \frac{\pi}{4}\, d_i^2\, q'''_f}{\frac{\pi}{4}\, d_i^2\, v\, \rho\, C_p}\, L \,, \tag{11.4-9}$$

where d_o is the tube outer diameter, C_p is the specific heat capacity of the coolant, and q'''_w, q'''_a, and q'''_f are the volumetric heating rates in the tube wall, armor, and coolant, respectively. The surface heat flux in Equation 11.4-9 is averaged between the inboard and outboard locations.

A 1-D thermal analysis is performed at the location of the coolant tube outlet to estimate the peak temperatures in the target. The temperature drops through the boundary layer, ΔT_f, the tube wall, ΔT_w , and the armor, ΔT_a, are given by

$$\Delta T_f \;=\; \frac{q''_c}{h} \,, \tag{11.4-10}$$

$$\Delta T_w \;=\; \frac{q''\, d_o}{2k_w} \ln\left(\frac{d_o}{d_i}\right) + \frac{q'''_w\, d_o^2}{8k_w} \ln\left(\frac{d_o}{d_i}\right) - \frac{q'''_w}{16k_w}\left(d_o^2 - d_i^2\right) \,, \tag{11.4-11}$$

$$\Delta T_a \;=\; \left(q''_{sur} + \frac{t_a}{2}\, q'''_a\right) \frac{t_a}{k_a} \,, \tag{11.4-12}$$

where k_w and k_a are the thermal conductivities of the tube wall and the armor, respectively, and t_a is the minimum thickness of the armor. The heat flux term in the expression for the wall temperature drop, Equation 11.4-11, includes an allowance for the volumetric nuclear heating in the armor, which also must be conducted through the tube wall.

The heat fluxes used in Equations 11.4-10 to 11.4-12 refer to the coolant outlet location. The heat flux at this location is lower than the inboard/outboard average, because the coolant outlet header is 45° above the outboard midplane of the machine and the toroidal geometry leads to a reduction in heat flux on the divertor target with increasing major radius.

The peak temperatures in the vanadium-alloy tube wall, $T_{w,max}$, and in the tungsten-alloy armor, $T_{a,max}$, are determined from

$$T_{w,max} = T_{ex} + \Delta T_f + \Delta T_w \qquad (11.4\text{-}13)$$

$$T_{a,max} = T_{w,max} + \Delta T_a \,. \qquad (11.4\text{-}14)$$

The values for the materials properties were given in Table 11.2-I in Section 11.2.5. Design parameters for the thermal analysis are given here in Table 11.4-I.

11.4.3. Design Parameters

For the final design of the target, the following constraints were imposed. A 0.5-mm-thick coolant-tube wall was chosen rather then the 1-mm thickness used for the first-wall tubes because of the higher heat fluxes in the divertor; the reduced thickness is possible because the tube is protected from potential sputtering damage by the tungsten-alloy armor. The diameter of the tubes is reduced by the same factor to ensure that the pressure stress does not increase. The coolant inlet temperature of 320 °C is the same as for the first wall, allowing both coolant loops to be fed from the same circuit. Allowance is made in the thermal calculations for the temperature increase associated with the deposition of the pumping power into the coolant.

The maximum allowable coolant velocity was set at 25 m/s for this analysis, based on considerations of physical erosion (Section 10.2). This velocity is only slightly greater than that of the first-wall coolant which is ~ 21 m/s. While, it is desirable that the total pressure drop in the divertor coolant to be about the same as that of the first-wall coolant circuit (10 MPa), this design convenience did not appear possible, and a total pressure drop of 12 MPa was used for the divertor-coolant circuit. Since substantial

Table 11.4-I.

DESIGN PARAMETERS FOR THERMAL ANALYSIS

Thickness of W-Re armor, t_a	2.0	mm
V-alloy tube-wall thickness, t_w	0.5	mm
V-alloy tube inner diameter, d_i	5.0	mm
Nuclear heating rate in armor, q_a'''	100	MW/m^3
Nuclear heating rate in tube wall, q_w'''	100	MW/m^3
Nuclear heating rate in coolant, q_f'''	100	MW/m^3
Coolant inlet temperature, T_{in}	320	°C
Maximum allowable coolant velocity, v_{max}	25	m/s
Total coolant pressure drop, ΔP	12	MPa
Maximum allowable V-alloy temperature, $T_{w,max}$	750	°C

simplifiction results from cooling two components (first wall and divertor) from the same cooling circuit, it is assumed that a 12-MPa pump would be used for both components, and the excess pressure for the first wall circuit would be removed with an orifice.

The final geometry of the divertor, representing the converged solution to the divertor design problem described above, is shown in Figure 11.4-1. This figure contains views of both the inboard and outboard sections, illustrating the more compressed geometry on the inboard side, which arises because of toroidal effects and the inverse major radius dependence of the toroidal field. The closeness of the null point to the divertor plate surface ($\sim$ 1 cm) is clear from the figure, but neutral-atom transport calculations indicate that a negligibly small fraction of the particles released from the target re-enters the core plasma (Section 5).

Figure 11.1-1 shows a large gap between banks of TF IBCs in the divertor region. In Figure 11.4-1 much of this space has been filled with identical, but non-current-carrying, poloidal tubes of liquid lithium. This additional tubes improve the blanket coverage and the tritium breeding ratio (TBR), although 3-D neutronics calculations indicate that this

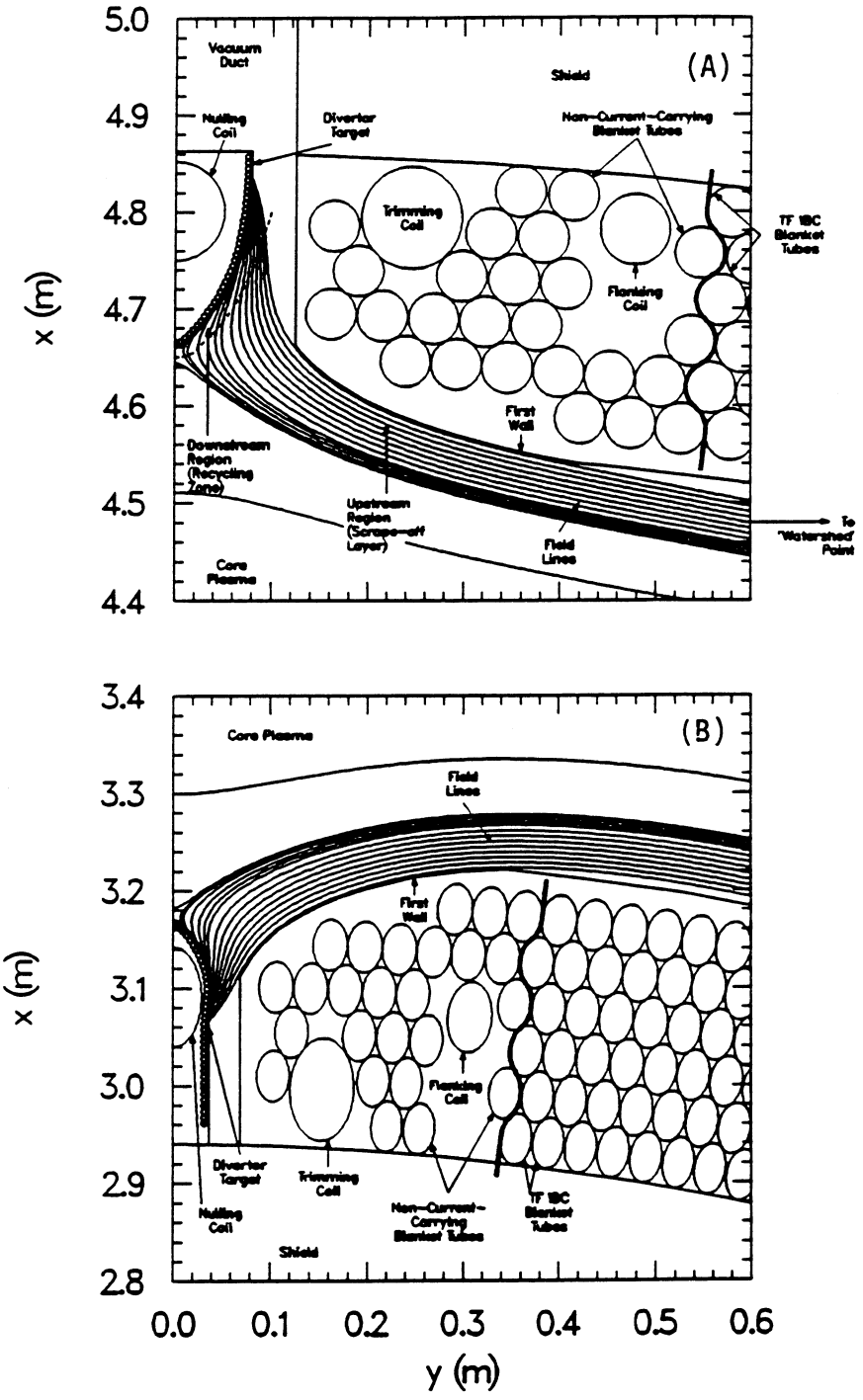

Figure 11.4-1. Outboard (A) and inboard (B) equatorial-plane views of the divertor region for TITAN-I.

is not necessary to achieve a TBR in excess of unity, nor to provide adequate shielding for the ohmic-heating (OH) coils (Sections 10.3 and 11.7).

Also shown on the outboard view of Figure 11.4-1 is the pumping aperture which leads to the vacuum tank surrounding the torus. This aperture is present for only the outboard 90° in poloidal angle; elsewhere shielding material is provided to protect the OH coils. The positioning of the divertor coils within the envelope defined by the blanket ensures adequate shielding of the inner OH coils.

Figure 11.4-2 shows the distribution of the various components of the surface heat flux along the divertor target for the inboard and outboard locations. The heat flux is plotted for each coolant tube; tube number 0 is located on the apex of the target, which is directly in line between the nulling coil and the plasma centerline.

The heat flux on the inboard target is significantly higher than that on the outboard, because of the toroidal effects noted earlier. The peak heat fluxes are ~ 9.5 and $\sim 6\,\mathrm{MW/m^2}$ on the inboard and outboard targets, respectively. However, the maximum structural temperatures occur at the coolant outlet location (close to the outboard position), because the coolant temperature rise from inlet to outlet is the most significant factor. The maximum value of the inboard/outboard-averaged heat flux is about $7.5\,\mathrm{MW/m^2}$.

No plasma is incident on the target near its apex, since this region lies between the two points where the separatrix intersects the target. This region is heated only by radiation from the core plasma, and consequently there is a reduction in the surface heat flux at this point.

Corresponding to the increased heat flux on the inboard target, there is a reduction in the size of the heated region on the inboard side. Consequently, many of the coolant tubes are heated only along a portion of their length, since the tubes are of constant cross section. It is noteworthy that about 30% of the total heating rate is associated with the radiation from the core, edge, and divertor plasmas, illustrating the importance of including these components of the heat flux.

Figures 11.4-3 and 11.4-4 show plots of the flux-expansion factor, the inclination angle of the target with respect to the field lines, and the perpendicular (toroidal and radial) magnetic field strength. The structural temperature at certain points through the target is also shown in Figure 11.4-4 as a function of position along the target at the coolant outlet location. These figures show how the inclination angle was adjusted to maintain an acceptable heat flux along the target, given the varying values of the flux expansion factor and the magnetic field. Of particular importance is the strong variation of the magnetic

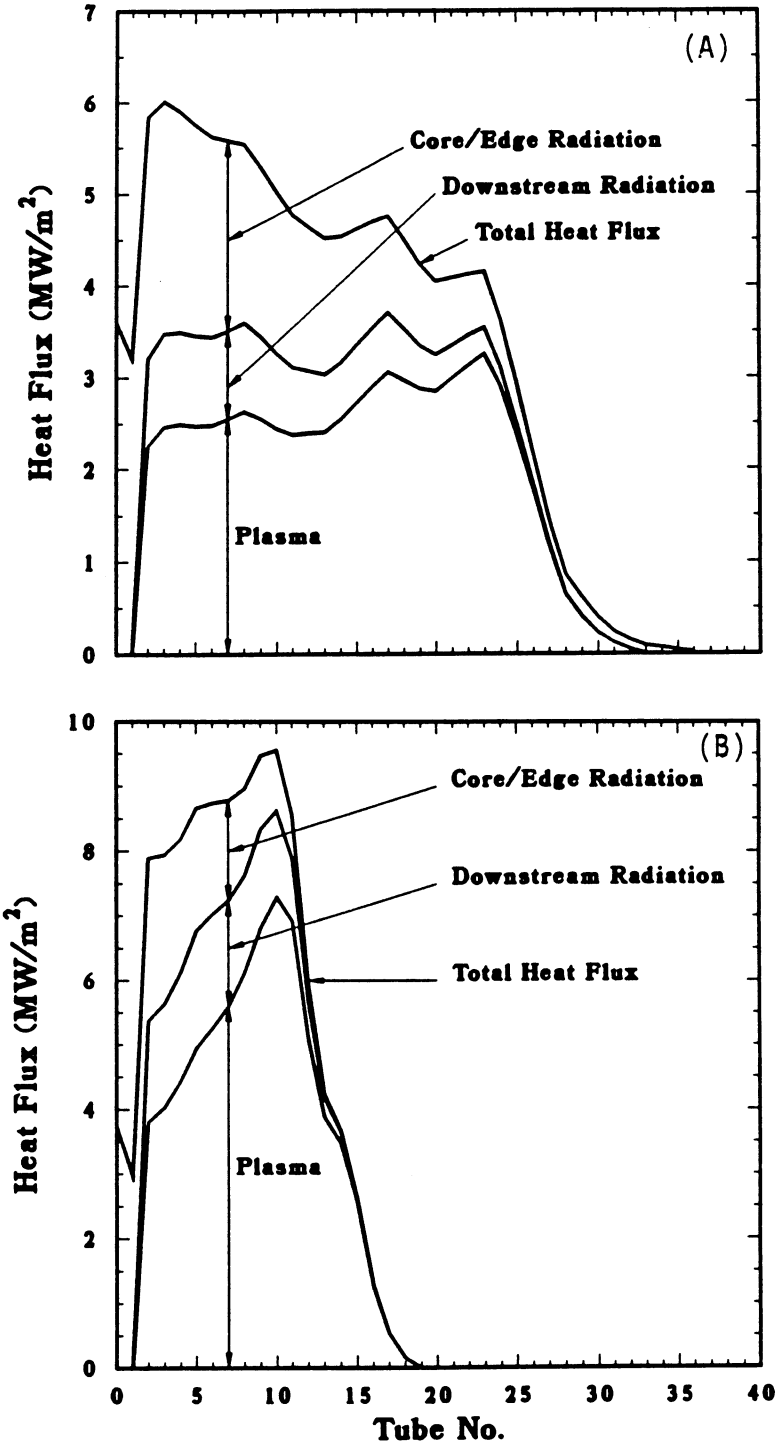

Figure 11.4-2. Heat flux distribution on outboard (A) and inboard (B) sections of divertor target. Coolant tubes are numbered from the apex or symmetry point of the target between the nulling coil and the core plasma.

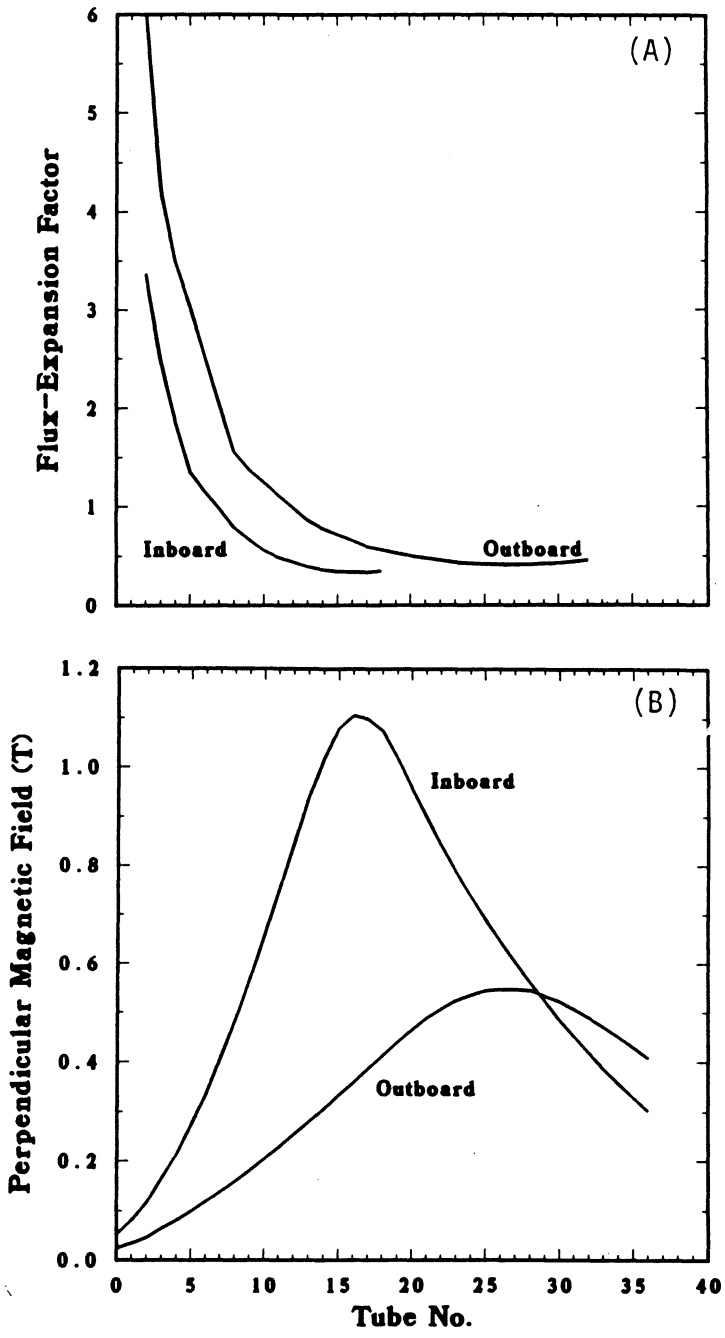

Figure 11.4-3. Flux-expansion factor (A) and perpendicular magnetic-field strength (B) as functions of position on inboard and outboard sections of divertor target. Coolant tubes are numbered from the apex or symmetry point of the target between the nulling coil and the core plasma.

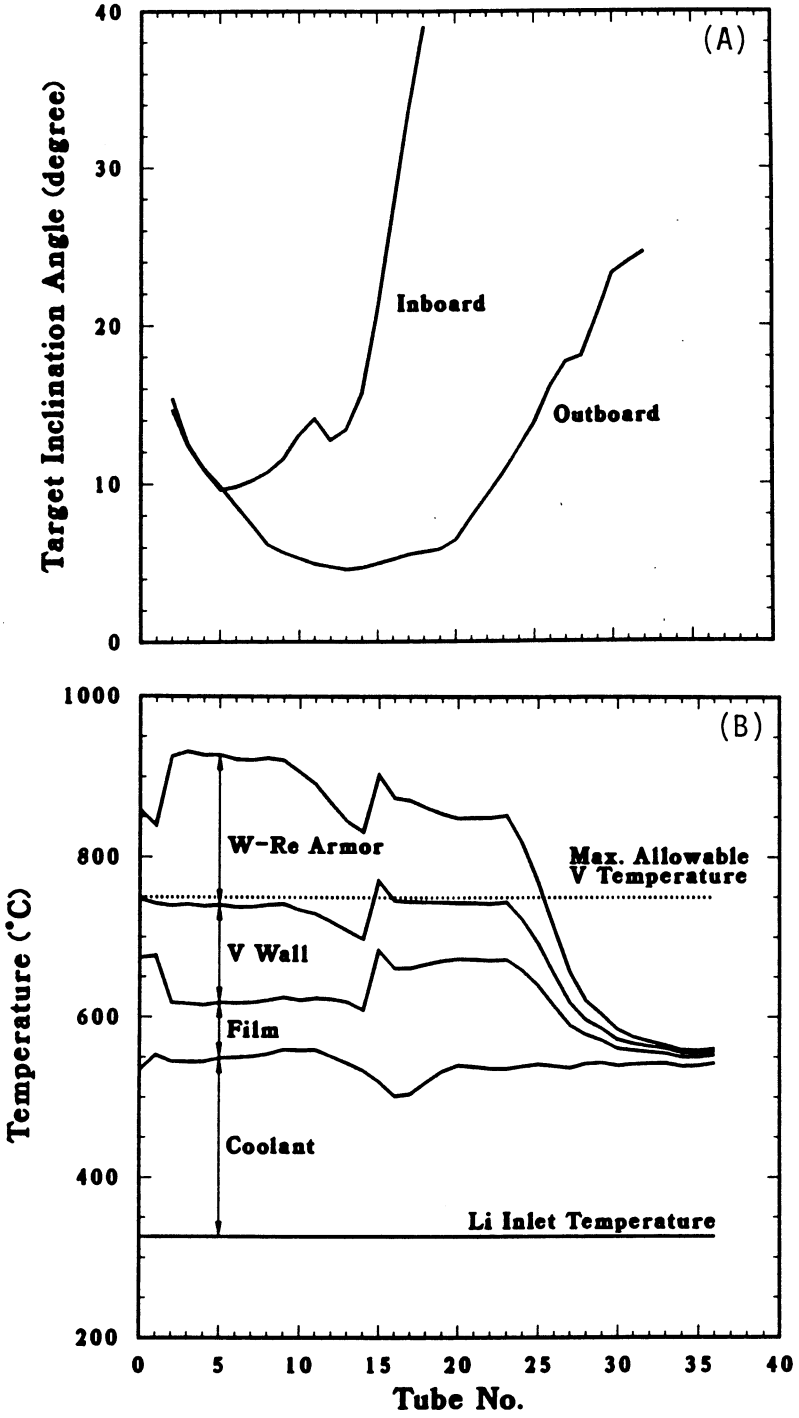

Figure 11.4-4. Target inclination angle (A) and coolant and structural temperatures at the coolant outlet (B) as functions of position on inboard and outboard sections of divertor target. Coolant tubes are numbered from the apex or symmetry point of the target between the nulling coil and the core plasma.

field; its low magnitude near the point where the separatrix intersects the target (and where the plasma heat flux is near its peak) allows high coolant velocities to be attained without excessive MHD pressure drops.

One of the most important constraints imposed on the target design is the 750 °C-maximum temperature of the vanadium-alloy tubes. Figure 11.4-4 shows that this condition is satisfied for all points on the target except for two tubes. At this location the curve for the film temperature drop shows a sharp spike, which is caused by a sudden transition from the turbulent to the laminar regime, as is given by the criterion in Equation 11.4-7. It is likely that a gradual transition would be achieved in practice, implying that the temperature estimate is conservative. In any case, the temperature exceeds the limit by only $\sim 10\,^{\circ}\mathrm{C}$, which is not considered significant. The maximum temperature of the tungsten-rhenium armor is about 930 °C, at which level the alloy retains its high strength, and the thermal stresses are within allowable levels (Section 11.5).

Flow orificing is used extensively to tailor the coolant velocity distribution. In low-field regions, the large pressure head of 12 MPa would otherwise cause the velocity to exceed the 25 m/s limit. Near the outside of the plate, orificing allows the coolant outlet temperature to be adjusted in order to maintain an approximately constant level across the plate. These features are illustrated in Figures 11.4-5.

A more extensive structural and thermal analysis of the divertor target using finite-element techniques is reported in the next section.

11.5. THERMAL AND STRUCTURAL ANALYSIS

In order to achieve the desired one year lifetime, the TITAN-I divertor must satisfy three major criteria:

1. Low erosion, which is accomplished by using tungsten as the plasma-facing material and ensuring a low-enough plasma temperature at the target;
2. Acceptable stresses, as dictated by the ASME Boiler and Pressure-Vessel Code;
3. Acceptable temperature, and of particular importance, the maximum temperature limit of 750 °C for the vanadium tubes.

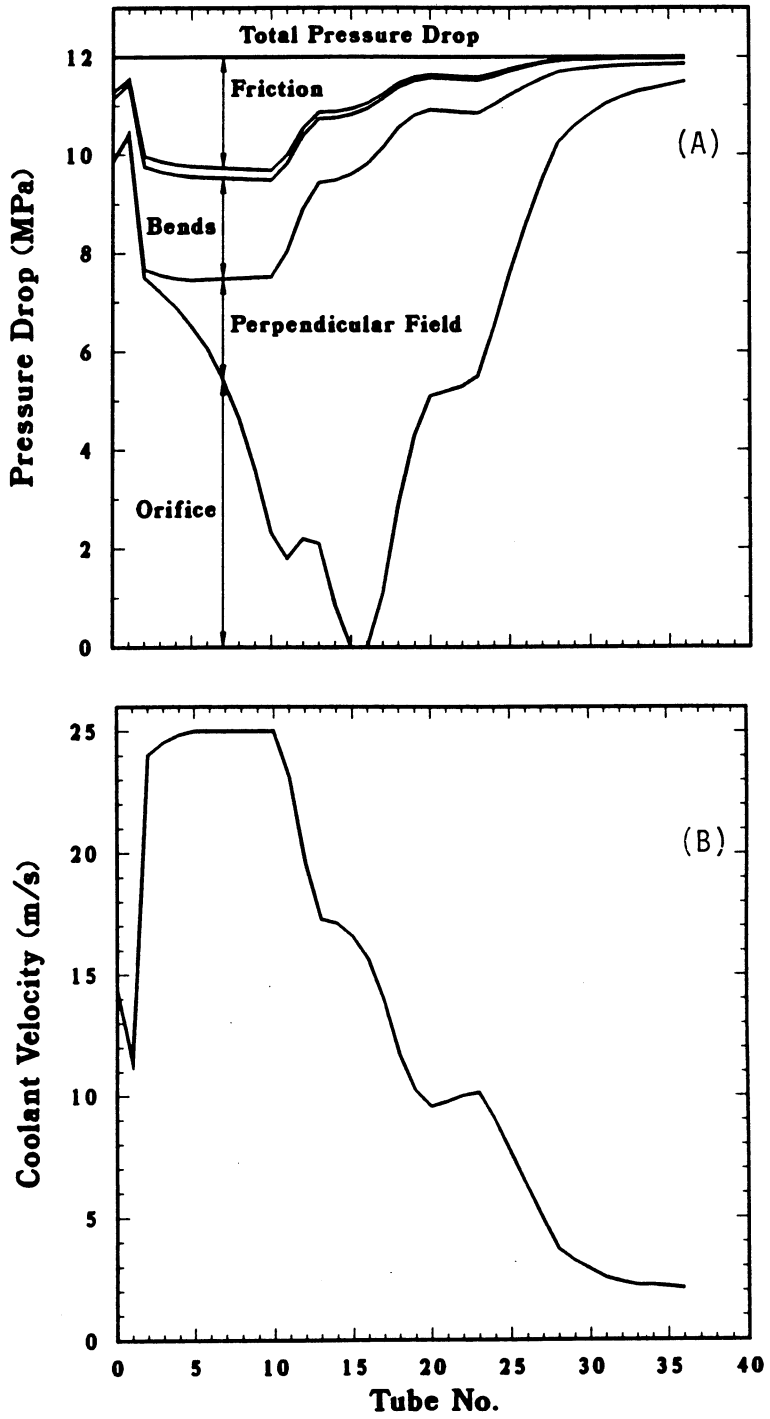

Figure 11.4-5. Components of the coolant pressure drop (A) and distribution of coolant velocities (B) for coolant tubes in the divertor target. Coolant tubes are numbered from the apex or symmetry point of the target between the nulling coil and the core plasma.

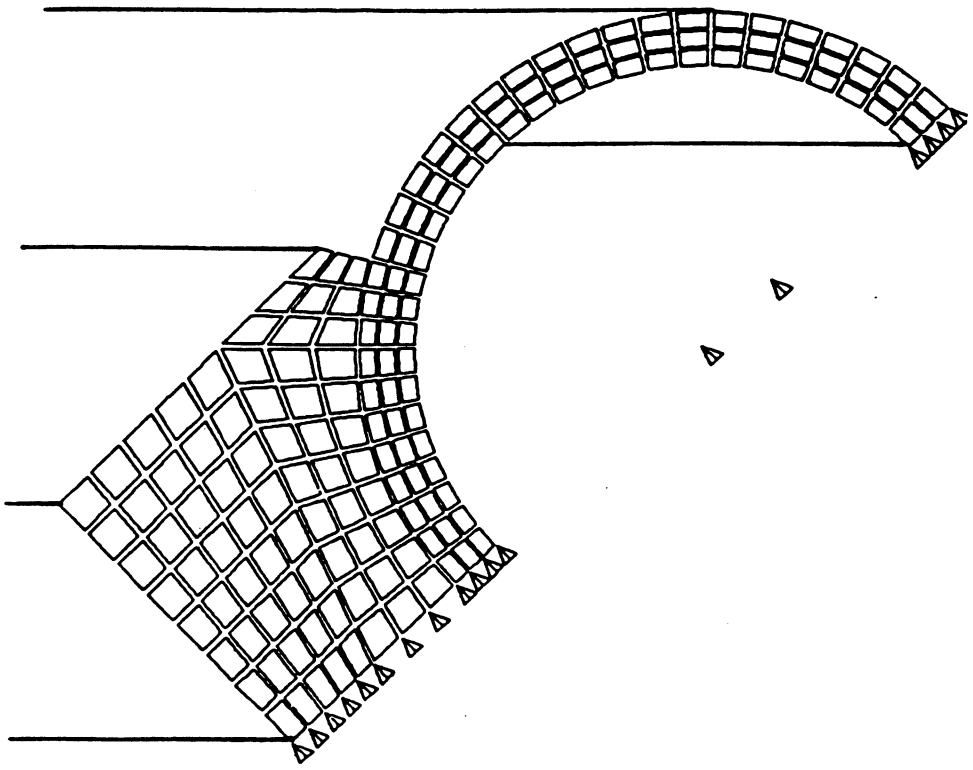

Figure 11.5-1. Finite-element model for thermostructural analysis of the divertor plate.

Estimates of the erosion rate for TITAN-I divertor target were discussed in Section 5.5, and an approximate thermal analysis was described in Section 11.4. A detailed finite-element analysis of the steady-state temperatures and stresses in the divertor plate is reported in this section.

The steady-state temperatures and stresses in the divertor were calculated using ANSYS [17], a widely used finite-element code. Because of the double curvature of the tungsten plate, a complete finite-element model is difficult and costly to construct, so an approximate 2-D model was used to allow a detailed study of the interface between the tungsten and the vanadium. The critical location for the divertor would be at the coolant outlet, near the outboard side, where the maximum temperatures are expected to occur. The peak heat flux at this location is $6.3\,\mathrm{MW/m^2}$. This portion of the divertor is modeled by assuming poloidal axisymmetry and using symmetry to model the structural behavior between neighboring tubes. The model, shown in Figure 11.5-1, consists of 135 quadrilateral elements. The material properties used in the analysis are given in Table 11.5-I.

Table 11.5-I.

MATERIAL PROPERTIES USED IN THERMOSTRUCTURAL ANALYSIS OF THE TITAN-I DIVERTOR

	Vanadium	Tungsten
Young's modulus, E (MPa)	114	385
Poisson's ratio, ν	0.36	0.3
Thermal-expansion coefficient, α (10^{-6}/K)	10	8
Thermal conductivity, k (W/m K)	29	67
Allowable stress, S_{mt} (MPa)	108 (650 °C)	200 (650°C)

11.5.1. Thermal Analysis

The heat flux on the divertor armor was assumed to be constant at 6.3 MW/m^2. Heat transfer into the coolant was modeled assuming a constant heat-transfer coefficient of 81 kW/m^2 K and all the other surfaces were assumed to be adiabatic. The coolant bulk temperature at this point is $\sim$ 540 °C.

The temperature contours for this model are illustrated in Figure 11.5-2, which shows that the temperature distribution in the tungsten armor is approximately one dimensional and little conduction to the rear of the tube is observed. The peak temperatures are 720 and 922 °C in the vanadium tubes and the tungsten armor, respectively, in good agreement with the results for an equivalent location in the approximate model (Figure 11.4-4). Each of these values is below the allowable limit.

11.5.2. Pressure Stresses

The equivalent primary stresses, induced by the 12-MPA coolant pressure are shown in Figure 11.5-3. Note that this calculation is conservative because the pressure will be significantly lower than 12 MPa at the coolant outlet location. The stresses in the vanadium are similar to those in a tube without a plate attached and the stresses in

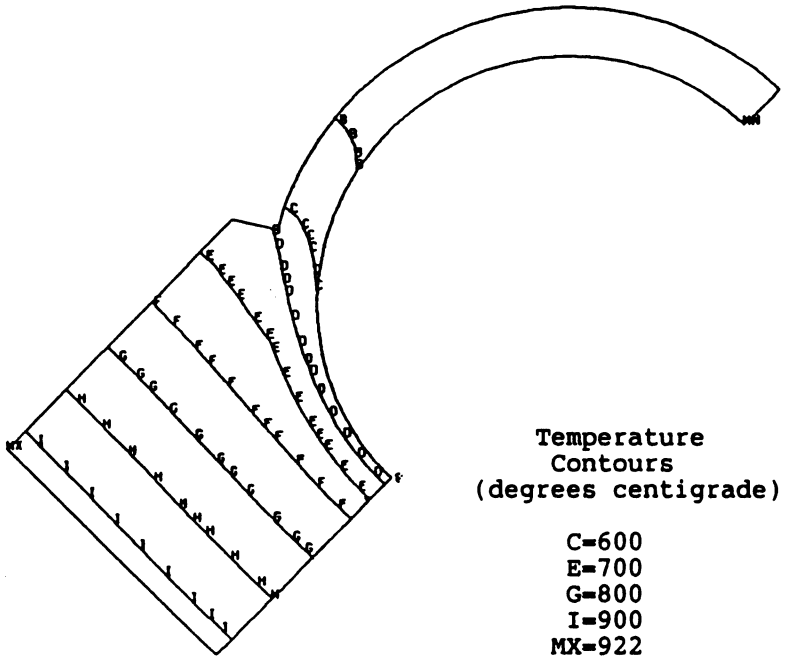

Figure 11.5-2. Temperature contours in TITAN-I divertor target for surface heat flux of 6.3 MW/m^2.

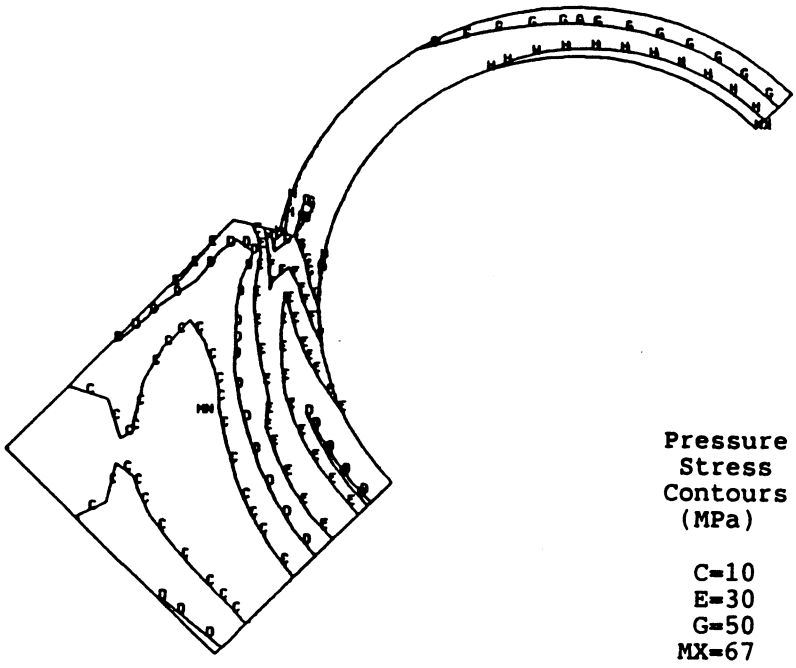

Figure 11.5-3. Contours of equivalent pressure in TITAN-I divertor target for coolant pressure of 12 MPa.

the tungsten are much lower. The peak stress in the vanadium is 67 MPa, which is well within the allowable value of S_{mt} of about 80 MPa at 700 °C.

11.5.3. Thermal Stresses

The equivalent thermal stresses in the divertor plate are induced by two key mechanisms: the temperature gradient and the differential expansion of the two materials. The temperature gradient causes stresses in the direction perpendicular to both the coolant flow and the heat flux. These stresses are similar to those caused by a uniform heat flux on a flat plate. The different thermal-expansion coefficients of the vanadium and tungsten alloys cause stresses in the bulk of the plate, as well as stress concentrations at the points where the interface intersects the free surface. Because of the need to satisfy both the equilibrium and compatibility equations near the traction-free intersection of the interface and component surface, these stress concentrations can be quite high. In fact, a purely elastic analysis would predict a stress singularity at this point, much like a typical stress field near the tip of a sharp crack in a fracture-mechanics analysis. If the singularity is assumed to be of the form $r^{-\delta}$, where r is the distance from the singular point, then δ, the order of the singularity, is usually 0.5 near a crack tip. The order of the singularity, however, is expected to be much smaller at about 0.1 for crack-free interface problems [18]. Because of the weakness of this singularity and the ability of plastic deformation to accommodate the deformations required by the compatibility equations without failure, the existence of a singularity in an elastic analysis cannot be used for design purposes until further testing is done. Hence, the stress concentrations determined from the finite-element analysis will be used to assess the viability of the TITAN-I divertor.

The equivalent thermal stresses in the divertor are shown in Figure 11.5-4. Except for the stress concentrations at the edge of the interface, the peak stresses are 400 MPa in the tungsten and 160 MPa in the vanadium. Each of these is within the allowable thermal stresses in the two materials. Near the edge of the interface, the peak reaches nearly 480 MPa in the tungsten, which is still within the allowable value of 600 MPa.

11.5.4. Global Deformations

One difficulty associated with the divertor target design is that accurate shaping of the plasma-facing surface is required to minimize the peak heat fluxes, as is discussed in Section 11.4. Because the divertor can easily undergo deformations and the null point

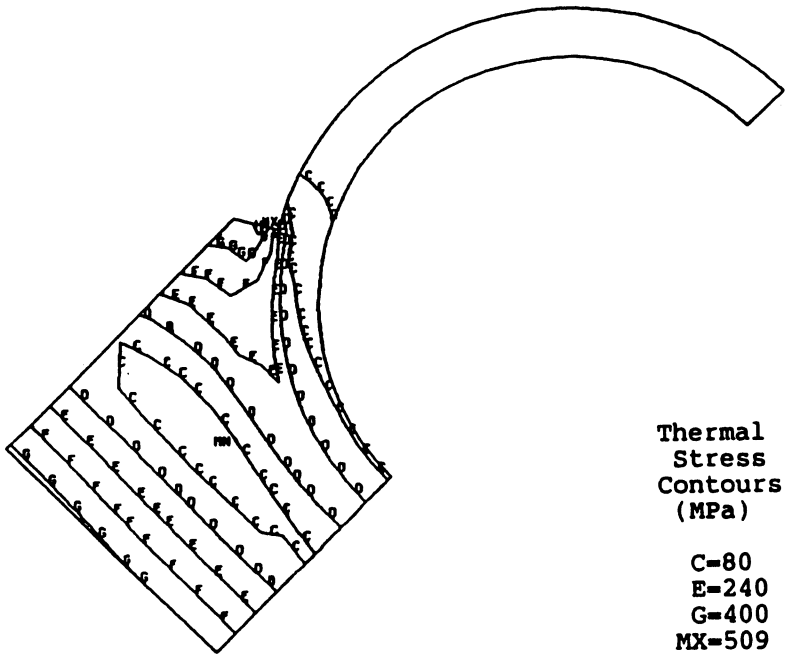

Figure 11.5-4. Contours of equivalent thermal stress in TITAN-I divertor target.

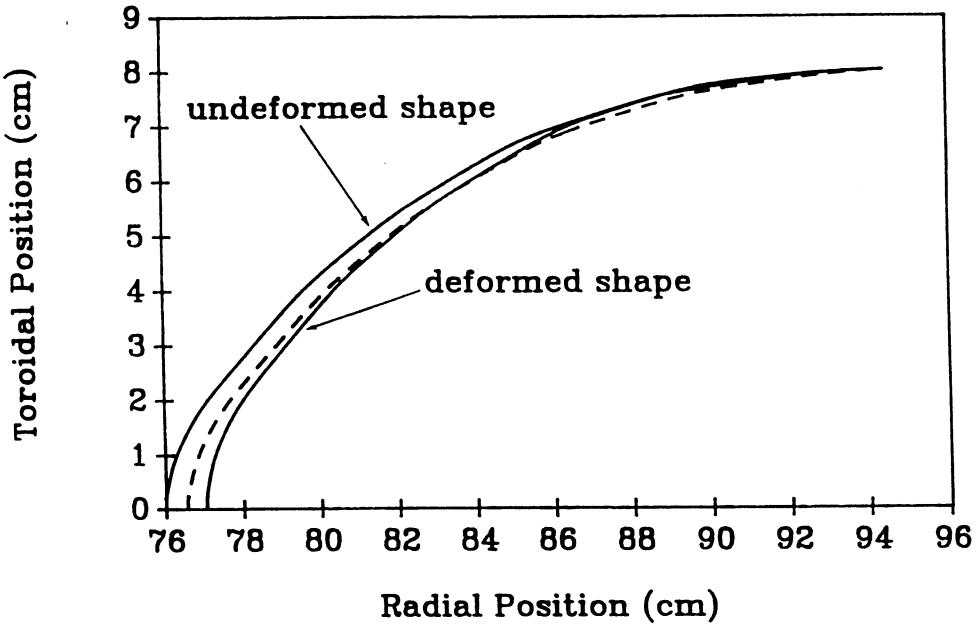

Figure 11.5-5. Initial and deformed shapes of the cross section of the TITAN-I divertor target, as compared with the desired deformed shape (dashed line).

is very close to the divertor target (about 1 cm), the initial shape of the tungsten plate must account for deflections induced during start-up, allowing an optimal shape during operation. An axisymmetric, finite-element model of the divertor cross section, ignoring the coolant tubes, was created to model the divertor deflections from the initial shape; the results are shown in Figure 11.5-5. The dashed line represents the desired deformed shape and the solid lines represent both the initial and final shapes of a particular design. The deformed shape is relatively close to the desired shape, but some alterations of the initial shape could achieve a closer tolerance, if it were required.

11.6. DIVERTOR COIL ENGINEERING

The TITAN-I divertor coils are based on the integrated-blanket coil (IBC) concept [2], in which an electrical current flows in a liquid-lithium coil, thereby combining the functions of magnetic field production, tritium breeding, and heat removal in a single system. This approach also eliminates the requirement for a shield in front of the divertor coils. Although the higher resistivity of lithium compared with that of copper causes higher joule heating, this energy is deposited in the primary coolant circuit and is recovered with the thermal efficiency of the energy-conversion system.

The magnetics design of divertor IBCs is presented in Section 4.4. Electrical engineering aspects of the TITAN-I divertor IBC are similar to that of the TF IBCs, therefore both are reported in Section 10.5. Forces on the divertor IBCs are of four types: (1) outward radial forces on each coil caused by the interaction of the coil current with the toroidal field, (2) centering forces resulting from the radial variation of the toroidal field, (3) overturning moments generated by the interaction between the vertical field and the IBC current, and (4) out-of-plane forces resulting from the spatial variation of the magnetic field especially in the divertor region. These electromagnetic forces also vary in time during the cycles of the oscillating-field current-drive (OFCD) system. The magnitude of these forces on divertor IBCs depends on the the reactor magnetic field and, therefore, they have been discussed in Section 10.5 and reproduced in Figure 11.6-1. This section focuses on the support structure needed to carry these loads.

The forces on the divertor coils are delineated in Section 10.5. Maximum loadings from the flank, trim, and nulling coils are presented in Figure 11.6-1 and show the structure design requirements. First, the five elements each have a simple solenoidal radial force which causes respective normal hoop tension, as is indicated. The resulting tensile stress in the coil material has significant effect on the remaining usable stress for the

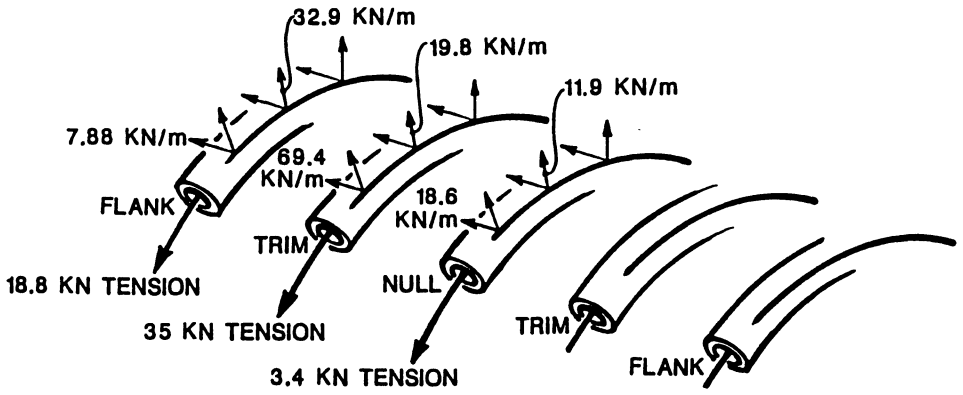

RESPECTIVE COIL FORCES (1), FORCE PER LENGTH OF COIL (2) AND MOMENT OF FORCE PER UNIT LENGTH OF COIL (3)

OVER-TURNING MOMENT (3)	NULL	TRIM	FLANK
	16 KNm/m	16 KNm/m	8.5 KNm/m
RADIAL* (2)	16→4 KN/m	40→60 KN/m	55→22 KN/m
LATERAL (1)	0	271.3 KN	3.5 KN

* VARIES AROUND COIL

Figure 11.6-1. Typical forces on TITAN-I divertor coils. Note that forces shown on the coils are reversed forces and the lateral and overturning-moment forces are combined. Design of the beam span is determined by the maximum combination of the radial and lateral-resolved forces.

bending loads as is described below. Second, the entire coil set has a tendency to move away from the center of the machine. These forces vary around each of the coils in the poloidal direction as their centers cross the spatially varying magnetic field and can be described as a single bursting force on the coil but of varying magnitude around it, as shown in the radial forces of Figure 11.6-1. Third, an overturning moment tends to twist the coil out of its plane. This moment is at a maximum at the top and bottom of the coils. Last, a lateral (toroidal) direction force on the coils tends to move them sideways. The null coil, which is on an axis of symmetry, is not subject to this force. It is important to note that these forces are time-varying during the cycles of the OFCD system.

The loads on the five divertor coils in each divertor module are too great to be cantilevered from the header and they should be supported. The support pitch is determined by the strength of the coil tubes and the loads imposed on them. The coil supports are embedded in the shield which is a 10-cm-thick vanadium-alloy shell. These supports transfer forces into the shell by means of ceramic compression pads which electrically insulate the assembly.

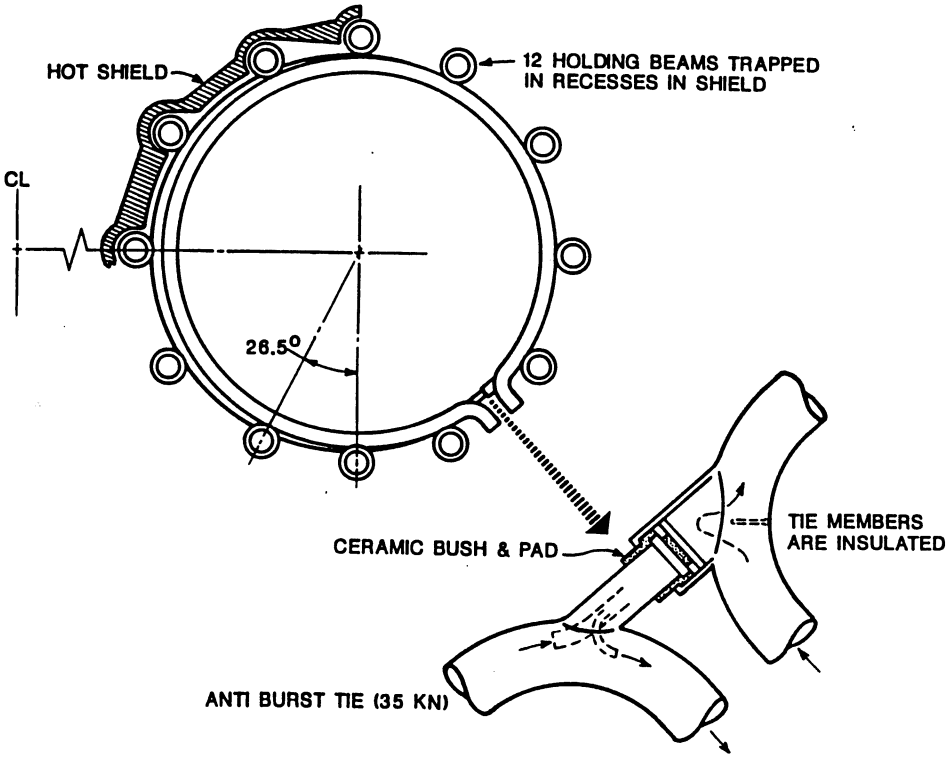

Figure 11.6-2. The restraint structure for the TITAN-I divertor IBCs.

The information on long-term or fatigue strength of irradiated vanadium alloys at high temperatures is inadequate at present. For the TITAN-I design, a value of 69 MPa (10 ksi) is assumed for a working stress. This stress, which is 10% of the room-temperature ultimate and two-thirds of the creep-rupture stress at operating temperature for one full-power year (FPY) of operation, allows 10^9 stress cycles. Figure 11.6-2 shows the adopted configuration for the support system. To support the hoop stress, an insulated tie is used to complete the coil near the header. The toroidal-direction support beams are not equally spaced. The loads at top and bottom are most intense and require a somewhat closer pitch.

Details of the coupling beam are shown in Figures 11.6-3 and 11.6-4. The beam is electrically connected only to the trim coils, having insulators at the null and flank coils and at the bearing pads which must transmit the loads on to the shield. Cooling of the coupling beam is accomplished by baffling some of the trim coil flow through the beam tube. Figure 11.6-4 shows additional baffling at the insulated connections to the null and flank coils to ensure cooling of the attachment point. Realization of this concept will undoubtedly require further development and experimental verification.

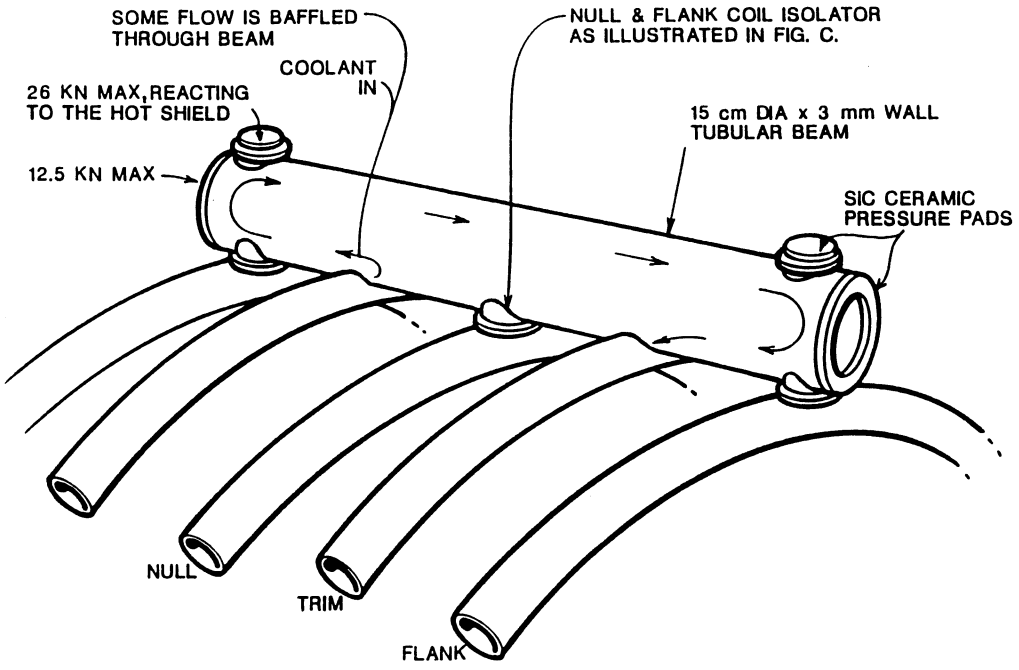

Figure 11.6-3. Coupling beam of the TITAN-I divertor IBCs.

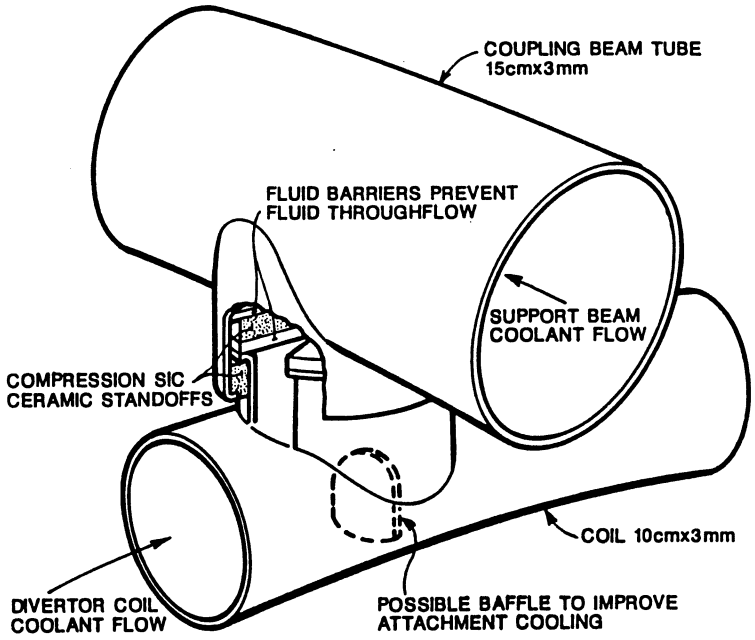

Figure 11.6-4. Insulated coil/beam attachment for the TITAN-I divertor IBCs.

11.7. NEUTRONICS

Nuclear heating and irradiation damage to the divertor IBCs are not different from those of the TF IBCs. The remaining issue is the radiation damage to the OH coils in the region behind the divertor, where the limited available space may lead to a more stringent requirement for shielding, particularly in the inboard region.

A 50-cm-thick reference shield design was adopted for the TITAN-I divertor region. The remaining 25-cm space between the first wall and this shield would then be available for the divertor IBCs and the collector plates; any shielding function provided by the material in this region was ignored for the purposes of this calculation. The composition of this divertor shield is 90% vanadium alloy and 10% lithium (30% enrichment in ^{6}Li). In this case, the fast-neutron fluence at the OH coil does not exceed $9.6 \times 10^{26}\,\mathrm{n/m^2}$, for 30 FPY of operation. This fluence is about a factor of 3 lower than the limit specified in Section 10.2 for the spinel insulator of the TITAN-I OH coils. When the divertor coils and the collector plates are included in the neutronics calculation, the fast-neutron fluence at the OH coil should be much lower than the value given above.

The lifetime of the shield was estimated assuming a limit of 200 dpa as the maximum damage allowed for the vanadium structural alloy. Using this criterion, the first 0.3 m of the shield nearest to the plasma must be replaced after every full-power year of operation, while the next 0.15 m will have a lifetime of 5 FPY. The nuclear heating rate at the OH coil is less than $2.8\,\mathrm{MW/m^3}$, which is similar to the rate in regions remote from the divertor, behind the blanket and hot shield.

After this reference design was completed, it became clear that it would be possible to incorporate some non-IBC blanket tubes in the space allocated for the divertor coils and collector plates, as shown in Figure 11.4-1. This design improves both the tritium breeding ratio and the energy recovered from the blanket. The non-IBC region is 0.28 m thick (as is the rest of the blanket and hot-shield design), although a larger void fraction exists, resulting in the composition of 10.8% vanadium, 43.2% lithium, and 46% void. The final divertor-shield design consists of two zones, located behind the non-IBC blanket tubes behind the divertor target region. The first zone is composed of 30% vanadium and 70% lithium, and a second zone consists of 90% vanadium and 10% lithium. Optimum thicknesses for these two shield zones were found to be 0.3 and 0.15 m, respectively, in order to limit the maximum fast-neutron fluence at the OH coil to about $9 \times 10^{26}\,\mathrm{n/m^2}$ after 30 FPY of operation. The lifetime for the non-IBC blankets, divertor coils, collector plates, and first shield zone is estimated to be 1 FPY, while the last 0.15 m of the shielding component, similar to that in the other design option, will last for 5 FPY.

Table 11.8-I.

ASSUMPTIONS FOR He AND DT REMOVAL DURING BURN

Throughput of DT	6.7×10^{21}	s^{-1}
Throughput of He	8.2×10^{20}	s^{-1}
Pressure in vacuum tank	20	mtorr
Temperature of neutral gas	700	K

11.8. VACUUM SYSTEMS

The vacuum system for TITAN-I is based upon a large vacuum tank surrounding the entire torus, OH coils, and the equilibrium-field (EF) coils. This approach is attractive because of the compact FPC of TITAN-I, which allows a relatively small tank ($\sim$ 16 m in diameter and 10 m high) to be used. The tank is connected to the plasma chamber via a pumping duct on the outboard side of the torus at each of the three divertor locations, as shown in Figure 11.4-1. The high vacuum pumps are situated outside the vacuum tank to allow easy access for maintenance. Pumping is performed through 12 ducts (one between each pair of EF-coil supports) which penetrate the tank. A general elevation view of the design is given in Figure 11.8-1.

11.8.1. Design Requirements

The requirements for the vacuum system design were assessed, considering both the removal of DT and He ash during the burn and initial pump-down of the plasma chamber. The configuration of the vacuum tank, pumping ducts, and vacuum pumps is shown in Figure 11.8-2. The main assumptions made in the calculations relating to the burn conditions are given in Table 11.8-I.

The particle throughputs are based on the results of plasma simulations described in Section 5.5. The vacuum-tank pressure is chosen to be compatible with the neutral-transport calculations for the divertor region. The pressure is estimated to be about

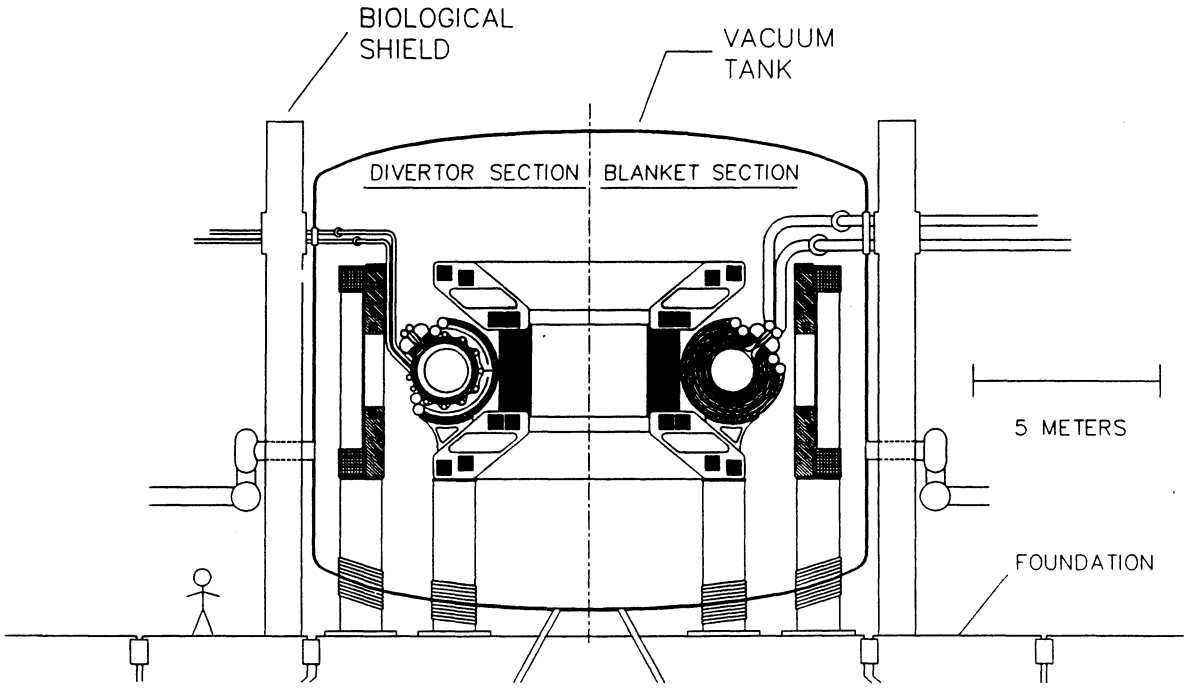

Figure 11.8-1. Elevation view of the TITAN-I FPC design, illustrating the geometry of vacuum tank.

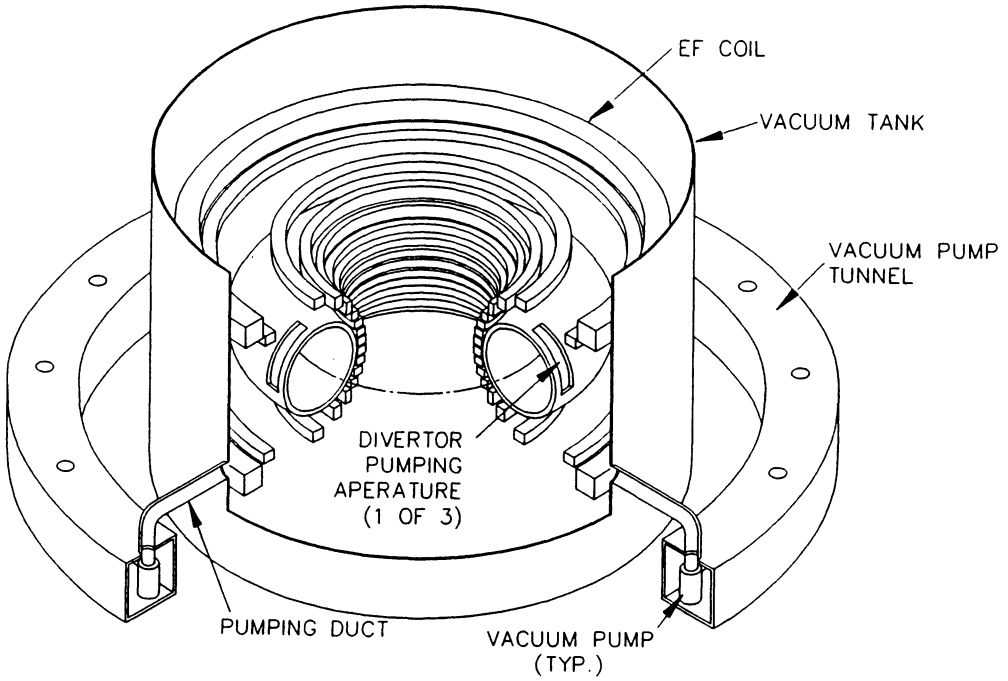

Figure 11.8-2. Configuration of vacuum tank, pumping duct, and vacuum pumps for the TITAN-I vacuum system.

20 mtorr; this pressure is sufficiently high that pumping speed requirements are not excessive. At these pressures, the gas flow is in the transition range between the regimes of molecular and viscous flow. Using standard prescriptions for vacuum-pumping calculations, incorporating Santeler's correction for molecular flow in short ducts [19], the net conductance of each duct is estimated to be $215\,m^3/s$ for DT and $224\,m^3/s$ for He. The resulting vacuum pumping speed required at each duct location is $21.8\,m^3/s$, or about $260\,m^3/s$ for the entire reactor.

The level of purity of the plasma chamber will be determined by the ultimate pressure than can be achieved with the vacuum-pumping equipment. An assessment of this issue was made by assuming outgassing to be the only source of impurities (*i.e.*, the vacuum tank is leak tight). An outgassing surface area equal to five times the inner plasma chamber surface and vacuum tank surfaces was used to account for the EF-coil case, blanket and shield, and various other exposed surfaces present inside the tank.

Outgassing rates of 10^{-7} to 10^{-8} torr liter/s cm^2 were considered, representing the range of values expected for baked stainless-steel surfaces. The minimum pumping speed required to achieve a base pressure of 10^{-8} torr in the plasma chamber ranges from 0.7 to $12\,m^3/s$ at each duct location. As this is less than that required for DT and He removal during the burn, pump-down to a reasonable base pressure appears not to be a serious concern for the TITAN-I design.

11.8.2. Vacuum Pumps

It is proposed to use magnetic-suspension-bearing turbo-molecular pumps for the high-vacuum pumps in TITAN-I. These pumps do not require oil lubricants, which can become contaminated with tritium or, if fluorocarbon oils are used, can cause fluoride corrosion of the pump. However, the largest model currently available has a pumping speed of only $2\,m^3/s$; in general, turbo-molecular pumps are limited to lower speeds than cryo-pumps. Manufacturers consider that higher speed pumps can be easily developed, and it is estimated that a turbo-molecular pump with a speed of $20\,m^3/s$ will only cost about a factor of 3.5 more (including development costs) than the largest which is currently available ($5\,m^3/s$) [20]. It is expected that pumps with a sufficiently high speed, such that the required number of pumps is not excessively large, will be available on the time scale envisioned for TITAN-I.

The magnetic field in the vicinity of turbo-molecular pumps must be less than a few hundred Gauss. To achieve this in a fusion facility which has relatively high magnetic

fields and requires close coupling of the pumps and vacuum tank, some magnetic shielding may be required. This shielding can be included in the pump housing outside the vacuum tank.

The other option for the high-vacuum pumps is to use compound cryo-pumps. Such pumps remove most gases by cryo-condensation and contain a sorption stage to remove helium. These pumps are already available at sizes sufficient for TITAN. The greatest drawback to their use is the high tritium inventory that accumulates within the pump between regenerations, which raises significant safety concerns and was the reason for preferring turbo-molecular pumps for TITAN.

Scroll pumps can be used to provide backing of the turbo-molecular pumps. These pumps, which employ a wobble rather than a rotary drive, are a sealed unit with no bearing lubricant exposed to tritium. Four $600\,m^3/h$ scroll pumps (one for every three duct locations), which can operate between atmospheric pressure and 50 mtorr, should provide adequate backing for this application.

11.9. SUMMARY AND CONCLUSIONS

The design of the impurity-control system poses some of the most severe problems of any component of a DT fusion reactor; for a compact or high-power-density device, these problems can be particularly challenging. For TITAN-I the impurity-control system is based on the use of toroidal-field divertors to minimize the perturbation to the global magnetic configuration, and to minimize the coil currents and stresses. Three such divertors are used as a compromise between the conflicting desires of minimizing the total ohmic losses in the divertor coils and maximizing the total area of divertor plates.

In order to maintain the heat flux on the divertor target plate at acceptable levels ($\leq 10\,MW/m^2$), the TITAN plasma is required to operate in a high-radiation regime, such that a total of about 95% of the steady-state heating power is radiated in the core, edge, and divertor plasmas. An "open" configuration, in which the divertor target is located close to the null point in the magnetic field, is used, rather than a "closed' configuration, which tends to produce large peaking factors in the heat-flux distribution. These features, together with careful shaping of the divertor target surface, allow the maximum heat flux at the inboard location to be restricted to $9.5\,MW/m^2$, with a peak outboard value of $6.0\,MW/m^2$.

To satisfy the requirement for a high-Z material for the plasma-facing surface of the divertor target, a tungsten-rhenium alloy (W-26Re) is proposed. The high rhenium

content provides the high ductility and high strength necessary for the severe loading conditions. A bank of lithium-cooled vanadium-alloy coolant tubes removes the heat deposited on the target; these tubes are separated from the tungsten-alloy armor by a thin, electrically insulating layer of spinel, to avoid an excessive MHD pressure drop. Fabrication of the divertor target is based on brazing of the tungsten-alloy plate (which is produced by powder-metallurgy techniques) to the bank of coolant tubes, with the spinel layer deposited by CVD process.

The low value of the toroidal field in the RFP allows high coolant velocities to be achieved without prohibitive MHD pressure drops, thus permitting operation in the turbulent flow regime, with the associated high heat-transfer coefficients. The maximum structural temperatures are $\leq 750\,^{\circ}C$ in the vanadium-alloy coolant tubes, and about $930\,^{\circ}C$ in the tungsten-alloy armor. A 2-D finite-element structural analysis indicated that stress concentrations will occur at the edge of the interface between the different materials of the target; this aspect requires further analysis and experimental investigation to ensure the viability of the design.

The vacuum system is based on the use of a large vacuum tank encompassing the entire torus, and connected to the divertor region by a duct located at each of the three divertor locations. Lubricant-free magnetic-suspension-bearing turbo-molecular pumps for the high-vacuum pumps are proposed to avoid the possibility of tritium contamination of oil lubricants. The pumps of the required size need to be developed.

In conclusion, at the present level of analysis, the toroidal-field divertor design for TITAN-I appears to represent a feasible design approach for the impurity-control and particle-removal system for a high-power-density RFP reactor. A number of areas require further analysis and experimental investigation to confirm their potential as described in this report. Demonstration of good RFP operation with a toroidal-field divertor is clearly necessary to justify the TITAN design. The use of a radiation-dominated plasma is central to the divertor design, and also requires further experimental work. The stress concentration which occurs at the boundary of the different materials needs further examination to ensure that the structural design is adequate, and the data base for the irradiated properties of the divertor target materials, especially the tungsten alloy, requires considerable expansion.

REFERENCES

[1] The NET Team, "NET Status Report," NET Report No. 51 (December 1985).

[2] D. Steiner, R. C. Block, and B. K. Malaviya, "The Integrated Blanket-Coil Concept Applied to a Poloidal Field and Blanket Systems of a Tokamak," *Fusion Technol.* **7** (1985) 66.

[3] W. D. Wilkinson, in *Properties of Refractory Metals,* Gordon and Breach Science Publishers, New York (1969).

[4] "Refractory Metals for Furnace Construction," Metallwerk Plansee GmbH Materials Brochure (1986).

[5] J. Hughes and G. Geach, "The Alloys with Molybdenum or with Tungsten and Having Good High-Temperature Properties," *Plansee Proc.* (1955), Pergamon Press Ltd., London (1956) 245.

[6] D. J. Maykuth, F. C. Holden, and R. I. Jaffee, "The Workability and Mechanical Properties of Tungsten- and Molybdenum-Base Alloys Containing Rhenium," in *Rhenium*, Elsevier, Amsterdam - New York (1962) 114.

[7] "Tungsten-Rhenium Alloys," in *Refractory Metals and Special Metals*, Metallwerk Plansee GmbH, Austria (1987).

[8] "How to Make Time with Tungsten," in *A Practical Guide on the Various Uses of Tungsten*, Schwarzkopf Development Corporation, Holliston, MA (1987).

[9] K. Verghese, L. R. Zumwalt, C. P. Peng, and T. S. Elleman, "Hydrogen Permeation through Non-Metallic Solids," *J. Nucl. Mater.* **112** (1979) 1161.

[10] K. Nateson, "Influence of Nonmetallic Elements on the Compatibility of Structural Materials with Alkali Metals," *J. Nucl. Mater.* **115** (1983) 251.

[11] D. L. Smith and K. Natesan, *Nucl. Technol.* **24** (1974) 64.

[12] G. Kneringer, K. Mayr, and R. Staffler, Metallwerk Plansee GmbH, Austria, private communications (1987).

[13] W. Kern and V. S. Ban, "Chemical-Vapor Deposition of Inorganic Thin Films," in *Thin Film Processes*, Academic Press, New York (1978) p. 257.

[14] F. A. Glaski, "A Report on the Current Role of Chemical-Vapor Deposition as a Manufacturing Process," *Proc. Conf. CVD of Refractory Metals, Alloys and Compounds*, Gatlinburg, TN (September 1967) 276.

[15] K. Suganuma, T. Okamoto, M. Koizumi, and M. Shimada, "Solid-State Bonding of Oxide Ceramic to Steel," *J. Nucl. Mater.* **117** (1985) 773.

[16] J. E. E. Baglin, "Adhesion at Metal-Ceramic Interfaces: Ion Beam Enhancement and the Role of Contaminants," in *Proc. of Mater. Res. Soc. Symp. on Thin Films: The Relationship of Structure to Properties*, San Francisco, CA (April 1985).

[17] G. J. DeSalvo and J. A. Swanson, "ANSYS Users' Manual," Swanson Analysis Systems, Inc. (1979).

[18] V. L. Hein and F. Erdogan, "Stress Singularities in a Two-Material Wedge," *Int. J. Frac. Mech.* **7** (1971).

[19] D. J. Santeler, "New Concepts in Molecular Gas Flow," *J. Vac. Sci. Technol.* **A4** (1986) 338.

[20] J. R. Haines, FEDC, Oak Ridge National Laboratory, private communication (June 1987).